J. Eur. Opt. Society-Rapid Publ. 2023, **19**, 1

https://doi.org/10.1051/jeos/2022014
Available online at: https://jeos.edpsciences.org

Journal of the European Optical Society-Rapid Publications

EOSAM 2022
Guest editors: Patricia Segonds, Gilles Pauliat and Emiliano Descrovi

REVIEW ARTICLE OPEN ACCESS

Comments about birefringence dispersion, with group and phase birefringence measurements in polarization-maintaining fibers

Thomas Villedieu[1], Laurent Lablonde[1], Hugo Boiron[2,3], Adrien Steib[1], Gilles Mélin[1], Thierry Robin[1], Benoît Cadier[1], Maxime Rattier[2], and Hervé C. Lefèvre[2,*]

[1] iXblue Photonics, Rue Paul Sabatier, 22300 Lannion, France
[2] iXblue, 34 Rue de la Croix de Fer, 78100 Saint-Germain-en-Laye, France
[3] Laboratoire Hubert Curien, UJM-CNRS-IOGS, 18 Rue Professeur Benoît Lauras, 42000 Saint-Etienne, France

Received 27 September 2022 / Accepted 27 November 2022

Abstract. A recent JEOS-RP publication proposed *Comments about Dispersion of Light Waves*, and we present here complementary comments for birefringence dispersion in polarization-maintaining (PM) fibers, and for its measurement techniques based on channeled spectrum analysis. We start by a study of early seminal papers, and we propose additional explanations to get a simpler understanding of the subject. A geometrical construction is described to relate phase birefringence to group birefringence, and it is applied to the measurement of several kinds of PM fibers using stress-induced photo-elasticity, or shape birefringence. These measurements confirm clearly that the difference between group birefringence and phase birefringence is limited to 15–20% in stress-induced PM fibers (bow-tie, panda, or tiger-eye), but that it can get up to a 3-fold factor with an elliptical-core (E-core) fiber. There are also surprising results with solid-core micro-structured PM fibers, that are based on shape birefringence, as E-core fibers.

Keywords: Birefringence, Birefringence dispersion, Channeled-spectrum analysis, Group birefringence, Phase birefringence, Polarization-maintaining fiber, Polarization-mode dispersion.

1 Introduction

A recent JEOS-RP publication proposed *Comments about Dispersion of Light Waves*, as well as simple geometrical constructions to relate group index n_g to phase index n, and it showed that these constructions can be extended to *phase* birefringence B and *group* birefringence B_g [1], that is noted as G, in some publications. Here, we propose a *complementary* paper to develop these comments and constructions for birefringence dispersion in polarization maintaining (PM) fibers.

We also present experimental measurements of group birefringence $B_g(\lambda)$ of several types of PM fibers over a wide spectrum range, knowing that it is quite easy today using a *supercontinuum* fiber source and *channeled spectrum analysis* with an optical spectrum analyzer (OSA).

We also show how to recover, from them, the value of phase birefringence $B(\lambda)$ over this wide spectrum, with a *single-wavelength* phase measurement $B(\lambda_0)$, since as it is well-known, phase birefringence measurements are not as easy to perform as group measurements. For these single-wavelength phase measurements, we use fiber Bragg gratings (FBG) and Rayleigh-OFDR (optical frequency domain reflectometry), and we explain why they measure phase birefringence.

As it will be shown, *unlike* the geometrical construction proposed in [1] that relates group birefringence $B_g(\lambda)$ to phase birefringence $B(\lambda)$, this requires now to relate phase birefringence $B(\lambda)$ to group birefringence $B_g(\lambda)$, to retrieve $B(\lambda)$ over a wide spectrum. A *reversed* geometrical construction is proposed for a *simpler* understanding ... in addition of some math, *we must admit*, since derivative, used to relate group to phase as seen in [1], is simple, whilst *integration*, needed to relate phase to group, yields firstly a primitive function (or indefinite integral), and then requires a *reference* at one wavelength to get a *definite* integral.

The preparation of this paper was also the opportunity to go back to early *seminal* papers on the subject. We may say that *everything*, or *almost* everything, that we are going to say can be found in the 1983 letter of Scott Rashleigh [2]. However, as you will see, this *great* three-page/one-figure letter deserves some *complementary* explanations, *to say the least*.

As the previous one [1], the present paper proposes many clear figures to ease the understanding, and it tries

* Corresponding author: herve.lefevre@ixblue.com

to avoid, *as much as possible*, complicated mathematical equations that might be not easily understandable.

2 Comments about early *seminal* papers

The first publication about the fabrication of what is called today *polarization-maintaining* (PM) fiber was by Stolen et al. in 1978 [3]. This fiber was based on stress-induced birefringence, and it was called a *high-birefringence* (HB, or also Hi-Bi) fiber since, as it was understood very early by Snitzer and Ostenberg [4], birefringence induces *phase mismatch* between both eigen polarization modes, which limits polarization degradation, since the various parasitic crossed couplings distributed along the fiber require *phase matching* to build efficiently a cumulative effect. This mismatch maintains a linear polarization that is coupled along one of the two principal axes of the high-birefringence fiber. These fibers were then called polarization-*preserving* [5], or polarization-*holding* [6]. It is amusing to see that the same coauthors of these two papers, Rashleigh and Stolen who are very important pioneers in the domain, *oscillated* between preserving and holding, in terms of vocabulary. In any case, they became subsequently polarization-*maintaining* (PM) fibers [7], which is the established vocabulary today.

The birefringence *strength* was originally given with the "*beat length*" (noted Λ)*, over which the relative phase difference between the two orthogonal modes changes by* 2π [3]. Even if it might sound obvious, it could be useful to remind that a classical bulk-optic half-wave plate has a thickness of half a beat length, and it is a quarter of beat length for a quarter-wave plate. This beat length was observed with *transverse* Rayleigh scattering [3, 8], which is working on the principle of a *dipole radio antenna* that cannot emit in a direction parallel to its axis. The equivalent of the antenna axis is the axis of the linear state of polarization. Like in a bulk crystal, launching a linear polarization at 45° of the principal birefringence axes yields a linear polarization that has been rotated by 90° after half the beat length, and that is back in the original direction after propagating along the whole beat length. Looking transversely at the fiber in the direction of the input polarization, there is no visible scattered light at the beginning, while there is scattering after half the beat length, since the polarization is now perpendicular to the direction of observation. One is back to no visible scattering after a full beat length since the polarization is parallel again. The fiber looks like a *glowing dashed line* [3], with a light-pattern periodicity equal to the beat length Λ (Fig. 1).

It is interesting to notice that this method is *still influencing* the vocabulary that is used today in the specification sheets of PM fiber manufacturers. Since the most common visible laser, *at that time*, was the helium–neon (He–Ne) laser, birefringence specification was, and is *still given*, with the beat length @ 633 nm, even if the operating wavelength is 1300 nm or 1550 nm! It is clear that the λ^{-4} dependency of Rayleigh scattering does not make this side-view observation as easy for near-infrared telecom wavelengths, as outlined by Rashleigh [2]. We shall see that phase birefringence B and group birefringence B_g, at the operating wavelength, are more relevant.

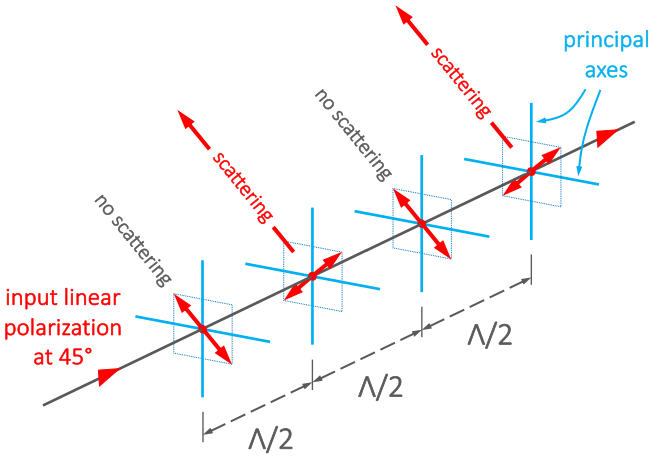

Figure 1. Principle of observation of the beat length, using *side viewing* of transverse Rayleigh scattering. Linearly polarized light is launched at 45° of the principal axes (blue lines) of the PM fiber, that appears as a *glowing dashed line* [3], with a periodicity equal to the beat length Λ.

The simple and classical method that is used today for measuring birefringence of PM fibers is derived from what was proposed independently by Rashleigh in 1982 [9] and by Kikuchi and Okoshi in 1983 [10]. It was called wavelength scanning [2], or wavelength sweeping [10], but it is actually based on what is known as interferometric *channeled spectrum* analysis, in courses of optics, like Born and Wolf [11]. A broadband light source is coupled at 45° of the principal axes of the *birefringent* PM fiber, and there is a second polarizer at the output, with the same 45° orientation. The output channeled spectrum is then measured with an optical spectrum analyzer, OSA (Fig. 2).

This forms a polarimeter that is equivalent to an unbalanced two-wave interferometer, considering the fast polarization mode as the short path, and the slow polarization mode as the long path. The polarizers at 45° are equivalent to the 50–50 spitters-recombiners of an interferometer, and the interferences are perfectly contrasted. The optical path length difference ΔL_{opt} is then:

$$\Delta L_{\text{opt}} = (n_{\text{eff}-\text{s}} - n_{\text{eff}-\text{f}}) \cdot L_f, \tag{1}$$

where L_f is the PM fiber length, $n_{\text{eff-s}}$ is the effective index of the slow (higher-index) mode, and $n_{\text{eff-f}}$ is the one of the fast (lower-index) mode. The phase birefringence B, also called *modal* birefringence, is given today with the difference between these effective phase indexes, as it is done in optics with birefringent crystals, such as quartz or lithium niobate:

$$B = \Delta n_{\text{eff}} = n_{\text{eff}-\text{s}} - n_{\text{eff}-\text{f}}. \tag{2}$$

There is a *bright* channel when ΔL_{opt} is an integer number m of the free-space wavelength $\lambda(m)$ that corresponds to this mth channel, i.e., when:

$$\Delta L_{\text{opt}} = (m-1) \cdot \lambda(m-1), \text{ or}$$
$$m \cdot \lambda(m), \text{ or } (m+1) \cdot \lambda(m+1). \tag{3}$$

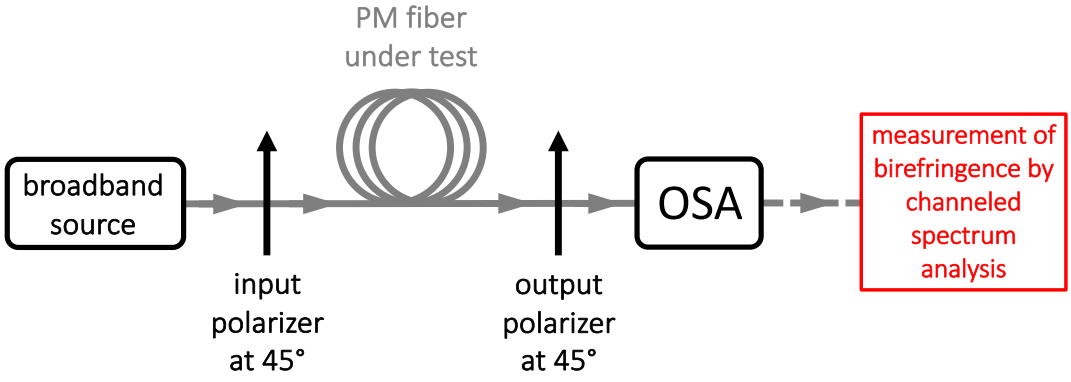

Figure 2. Principle of measurement of birefringence with channeled spectrum analysis: a broadband source light is sent into the PM fiber that is between polarizers at 45°, and this generates a channeled spectrum that is measured with an optical spectrum analyzer (OSA).

The integer $m-1$, or m, or $m+1$ is called the channel *order*. These bright channels are equally spaced in inverse of wavelength, i.e., in *spatial frequency* $\sigma(m) = 1/\lambda(m)$. The period of the spatial frequency spacing between adjacent bright channels is called the *free spectral range*, FSR_σ (Fig. 3). If one assumes that the birefringence B *is not dispersive*, i.e., that it does not vary with wavelength (or frequency), the result is very simple since, from (1) and (2), there is:

$$\begin{aligned}\Delta L_{\mathrm{opt}} &= B{\cdot}L_f = \Delta n_{\mathrm{eff}} \cdot L_f = m \cdot \lambda(m) \\ &= m/\sigma(m), \quad \text{and then}: \ \sigma(m) = m/(B \cdot L_f). \end{aligned} \tag{4}$$

Therefore, the free spectral range FSR_σ is:

$$\begin{aligned}\mathrm{FSR}_\sigma &= \sigma(m) - \sigma(m-1) \\ &= [m/(B \cdot L_f)] - [(m-1)/(B \cdot L_f)] \\ &= 1/B \cdot L_f \end{aligned} \tag{5}$$

and it yields a simple measurement of the birefringence B (Fig. 3). This birefringence B is related to the beat length Λ by:

$$B = \lambda/\Lambda \ \text{ and } \ \Lambda = \lambda \cdot \mathrm{FSR}_\sigma \cdot L_f. \tag{6}$$

This *assumption of dispersion-free* birefringence was done by Kikuchi and Okoshi in [10], as well as in an earlier Okoshi's paper of 1981 [12] and, very often, it is *still considered today.*

Notice that is also possible to perform this channeled spectrum measurement with a tunable laser and a power meter (Fig. 4).

Rashleigh made the same assumption in his 1982 letter [9], but *only* for PM fibers based on stress-induced photoelasticity. He was clear about the fact that *elliptical-core* (or E-core) PM fibers are *very dispersive*, as we will see later in this paper. In his *great* 1983 letter [2], he corrected reference [10], saying that channeled spectrum analysis *inherently measures group delay and not phase delay*, even for PM fibers based on stress-induced birefringence. However, he did not explain very clearly why. It was obvious to him ... but not obvious to us! As we will see in the following

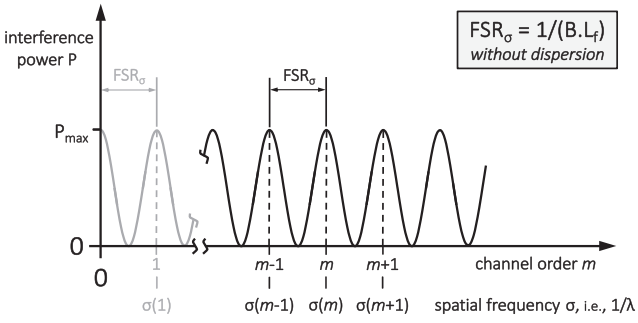

Figure 3. Principle of measurement of birefringence with channeled spectrum analysis: the measured free spectral range (FSR_σ) between two successive channels is equal to $1/(B \cdot L_f)$, in *absence* of dispersion. The first channel, displayed with a grey line, is *theoretical* since it corresponds to a quasi-infinite wavelength.

section, it is because the free spectral range, FSR, measured with channeled spectrum analysis, depends in fact on group birefringence B_g, and not on phase birefringence B. Group birefringence B_g is the difference between the *effective* group indexes of the two eigen modes [1]:

$$B_g = \Delta n_{\mathrm{g-eff}} = n_{\mathrm{g-eff-s}} - n_{\mathrm{g-eff-f}}. \tag{7}$$

With the term *delay* used by Rashleigh, one can notice that the vocabulary of that time was influenced by telecoms. Telecom scientists use *angular* frequencies to avoid the use of 2π in propagation equations. With this influence, phase birefringence was given [2, 9, 10, 12] as the difference $\Delta\beta$ between the propagation constant $\beta_s = 2\pi \cdot n_{\mathrm{eff\text{-}s}}/\lambda$ of the slow mode and $\beta_f = 2\pi \cdot n_{\mathrm{eff\text{-}f}}/\lambda$, the one of the fast mode. These propagation constants are the *effective* angular spatial frequencies (or wave numbers) of the two eigen polarization modes. In addition, free-space angular spatial frequency (or angular wave number), $k = 2\pi/\lambda$, was used, instead of the wavelength λ. If you look at the figure of Rashleigh's paper of 1983 [2], you see an angular wavenumber of 7.39 $\mu\mathrm{m}^{-1}$, which corresponds in fact to a wavelength of 0.85 µm, as said

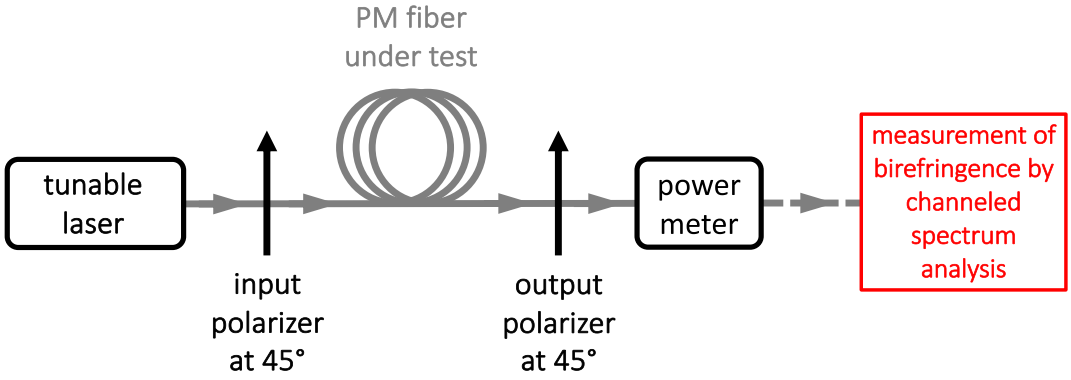

Figure 4. Principle of measurement of birefringence with channeled spectrum analysis, using a tunable laser and a power meter, instead of a broad-spectrum source and an OSA.

in the text, and the birefringence $\Delta\beta$ is given in cm^{-1}. It is not easily understandable since the radian unit is obviated. Radian being a dimensionless unit, it can be obviated *mathematically*, but this does not help the understanding, as it was shown in [1] for group velocity dispersion (GVD). A wavelength λ of 0.85 µm corresponds to a spatial frequency σ of 1.176 $\mu\mathrm{m}^{-1}$, and it is clearer to say that the angular spatial frequency or wave number k is 7.39 rad·$\mu\mathrm{m}^{-1}$ or rad/µm, i.e., 2π *radian* times 1.176 $\mu\mathrm{m}^{-1}$, rather than to have 7.39 $\mu\mathrm{m}^{-1}$ that has, then, the same unit as σ.

In addition, the use of $\Delta\beta$ to define phase birefringence as a function of k is not very convenient since:

$$\Delta\beta(k) = \Delta n_{\mathrm{eff}} \cdot k = B \cdot k. \tag{8}$$

Even with dispersion-free birefringence, i.e., when B is constant, $\Delta\beta(k)$ is not constant; it is proportional to k. As already seen, today, phase birefringence B is defined by the effective phase index difference Δn_{eff}. Without dispersion, this index difference is constant. The other advantage of the use of the index is that it is a *dimensionless* value, which avoids dealing with such *strange* units as cm^{-1}, obviating radian.

It is interesting to *revisit* the figure of Rashleigh's letter [2] of 1983 (Fig. 5). Following equation (8), the slope of the secant line that connects the origin to a point of the curve $\Delta\beta(k)$ is in fact the phase birefringence B, as it is defined today. A slope is a ratio, and when it is the ratio between parameters using the same *strange* unit … *strangeness* disappears!

Fiber A is a *bow-tie* fiber [13] that is based on stress-induced birefringence and has a phase birefringence $B = 5.2 \times 10^{-4}$, which is a typical value for industrial PM fiber products, today. Fiber B is a bow-tie fiber with lower birefringence (3×10^{-4}). Both have little dispersion since the slope varies only slightly when k is changing. Fiber C combines stress-induced birefringence with form birefringence, created by an elliptical core. It has a higher phase birefringence (7×10^{-4}) but, mainly, a much higher dispersion.

It is interesting to notice that equation (8) of Rashleigh's paper of 1983 [2] gives the *group delay time difference* τ_g between the two polarization modes:

$$\tau_g = (L_f/c) \cdot \mathrm{d}\Delta\beta/\mathrm{d}k, \tag{9}$$

where L_f is the length of the PM fiber. Today, τ_g is called differential group delay, or DGD. Since group birefringence B_g equates $\tau_g \cdot c/L_f$, there is:

$$B_g = \mathrm{d}\Delta\beta/\mathrm{d}k. \tag{10}$$

Group birefringence B_g is the derivative of $\Delta\beta(k)$ with respect to k, i.e., $\mathrm{d}\Delta\beta/\mathrm{d}k$ in Leibniz's notation, or $\Delta\beta'(k)$ in Lagrange's notation. Therefore, B_g is the slope of the tangent to the curve $\Delta\beta(k)$. Rashleigh's figure can be *revisited* again (Fig. 6). With fiber C, that is very dispersive because of its elliptical core, and choosing $\lambda = 1.3$ µm, i.e., $k = 4.83$ rad $\mu\mathrm{m}^{-1}$, as in Table 1 of [2], group birefringence B_g is 3.4 times phase birefringence B: 16×10^{-4} instead of 4.7×10^{-4}! Such an important difference will be confirmed with measurements of an elliptical-core (or E-core) PM fiber, later in this paper.

As we just saw, using $\Delta\beta$ as the definition of the birefringence has some *geometrical* interest with the use of the various slopes, but using Δn_{eff} is much simpler, and it is the common meaning of phase birefringence, today.

3 How to understand *simply* channeled spectrum analysis

As we just saw, an unbalanced interferometer yields a channeled spectrum with a bright channel when the optical path difference ΔL_{opt} is equal to an integer number m of free-space wavelength λ. In the case of a polarimeter, $\Delta L_{\mathrm{opt}} = B \cdot L_f = \Delta n_{\mathrm{eff}} \cdot L_f$, where L_f is the length of birefringent PM fiber under test. In the general case where there is a wavelength dependence of the phase birefringence B:

$$\Delta L_{\mathrm{opt}} = B[\lambda(m)] \cdot L_f = m \cdot \lambda(m), \tag{11}$$

$$m = B[\lambda(m)] \cdot [1/\lambda(m)] \cdot L_f, \tag{12}$$

where $\lambda(m)$ is the free-space wavelength that corresponds to the mth channel, and $B[\lambda(m)]$ is the phase birefringence

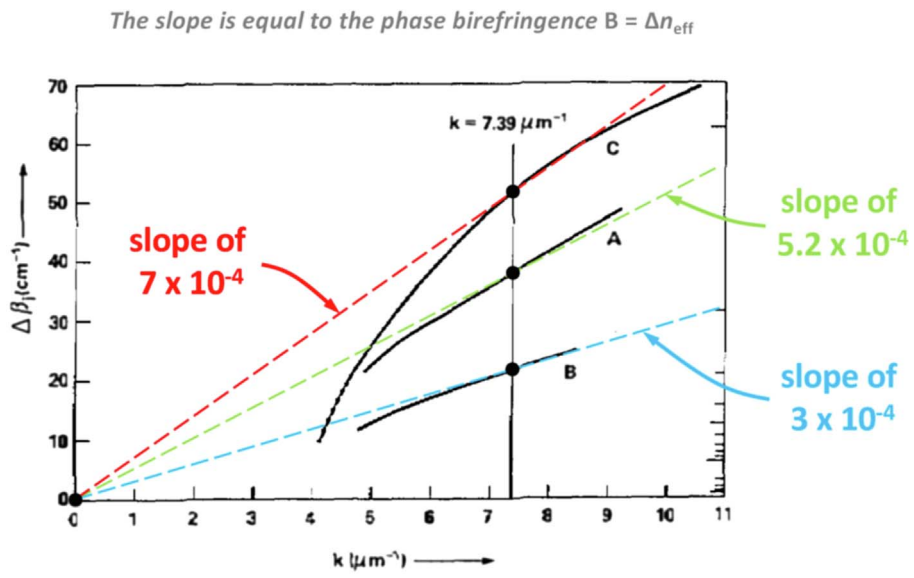

Fig. 1. Frequency dependence of the birefringence in the three high-birefringence fibers.

Figure 5. *Revisited* figure of Rashleigh's letter [2] of 1983: the slope of the various dashed secant lines in color is the phase birefringence $B = \Delta n_{\text{eff}}$, as it is defined today. Fibers A (green) and B (cyan) are *bow-tie* fibers. Fiber C (red) combines stress-induced birefringence with form birefringence. Free-space wavenumber k should be read 7.39 rad·μm^{-1}, and it corresponds to a wavelength λ of 0.85 μm.

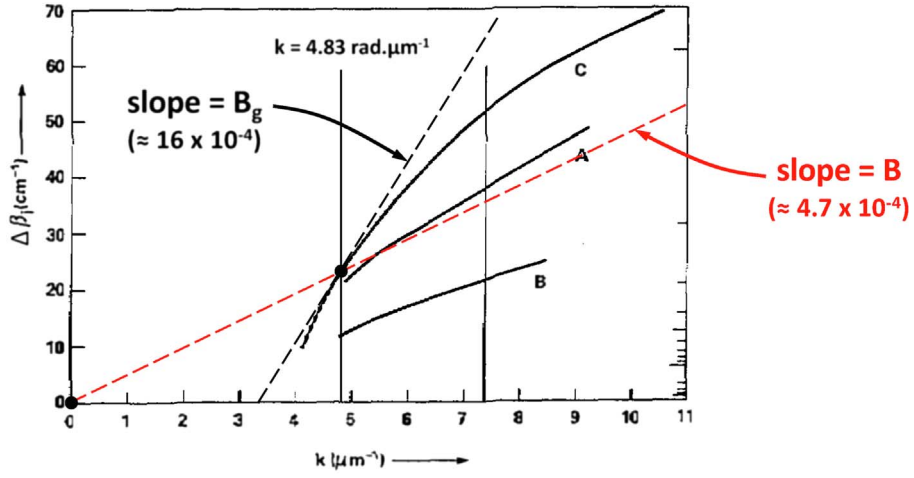

Fig. 1. Frequency dependence of the birefringence in the three high-birefringence fibers.

Figure 6. *Revisited* figure of Rashleigh's letter [2] of 1983: the slope of the tangent (black dashed line) to the curve $\Delta\beta(k)$ is the group birefringence B_g, as it is defined today. Fiber C is very dispersive: at $\lambda = 1.3$ μm, i.e., $k = 4.83$ rad·μm^{-1}, group birefringence B_g is 3.4 times higher than phase birefringence B!

of the PM fiber for this wavelength $\lambda(m)$. Using now the corresponding spatial frequency $\sigma(m) = 1/\lambda(m)$, there is:

$$m = \Delta L_{\text{opt}} \cdot \sigma(m) = B[\sigma(m)] \cdot \sigma(m) \cdot L_f. \qquad (13)$$

Mathematically, one can consider that the spatial frequency $\sigma(m)$ and the phase birefringence $B[\sigma(m)]$ are *continuous* functions of the parameter m, a bright channel corresponding to an integer value of m. With continuous functions, one can differentiate, and:

$$\mathrm{d}m = \mathrm{d}[B[\sigma(m)] \cdot \sigma(m)] \cdot L_f. \qquad (14)$$

As seen in equation (4) of reference [1], the group index n_g is the derivative of the *product* of the phase (or refractive) index n by the frequency. With the angular temporal frequency $\omega = 2\pi \cdot c/\lambda$, there is:

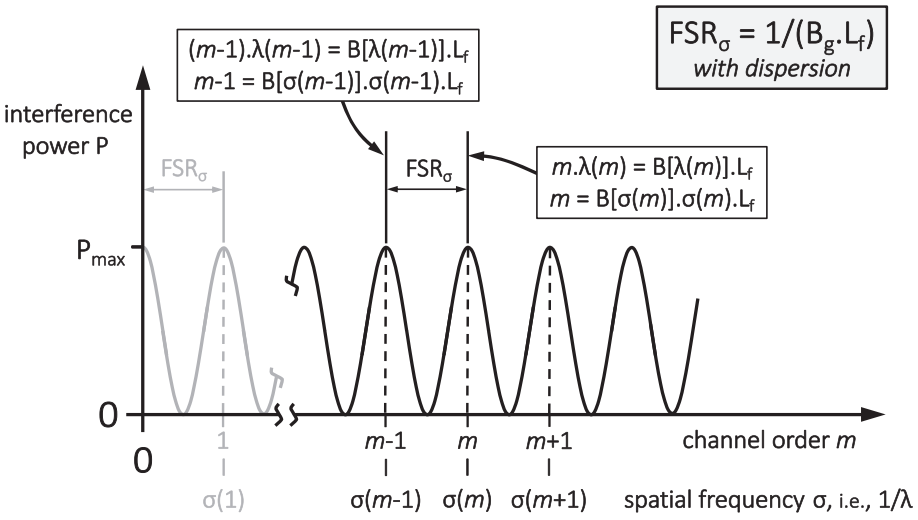

Figure 7. Principle of measurement of birefringence with channeled spectrum analysis, in the general case of birefringence dispersion. The free spectral range (FSR_σ), i.e., the spatial frequency difference between two successive bright channels, depends on group birefringence B_g: it is equal to $1/(B_g \cdot L_f)$. Theoretically, the position of the bright channels does depend on phase birefringence B, but there is no mean to measure it, since the channel order m cannot be known precisely without access to all orders down to zero frequency (grey line channel).

$$n_g(\omega) = \mathrm{d}[n(\omega) \cdot \omega]/\mathrm{d}\omega. \tag{15}$$

With the spatial frequency $\sigma = \omega/(2\pi \cdot c)$, since $\mathrm{d}\sigma/\sigma = \mathrm{d}\omega/\omega$, there is similarly:

$$n_g(\sigma) = \mathrm{d}[n(\sigma) \cdot \sigma]/\mathrm{d}\sigma. \tag{16}$$

Since the birefringence is the difference between the indexes of the polarization modes, for phase as well as for group, it simply yields:

$$B_g(\sigma) = \mathrm{d}[B(\sigma) \cdot \sigma]/\mathrm{d}\sigma. \tag{17}$$

Combining equations (14) and (17), one gets:

$$\mathrm{d}m = B_g \cdot \mathrm{d}\sigma \cdot L_f \text{ and } \mathrm{d}\sigma/\mathrm{d}m = 1/(B_g \cdot L_f). \tag{18}$$

The free spectral range in spatial frequency, FSR_σ, is the spatial frequency difference $\Delta\sigma$ corresponding to a parameter difference Δm that equates 1. Since $\Delta\sigma = (\mathrm{d}\sigma/\mathrm{d}m) \cdot \Delta m$, one gets:

$$\mathrm{FSR}_\sigma = \mathrm{d}\sigma/\mathrm{d}m = 1/(B_g \cdot L_f). \tag{19}$$

To summarize, the free spectral range FSR_σ depends on group birefringence B_g, and not on phase birefringence B, in the general case of birefringence dispersion. Theoretically, the *position* of the bright channels does depend on phase birefringence B, as seen in equation (13) but, in practice, there is *no mean* to know the precise value of the channel order m, since the broadband spectrum that is used remains limited. To have this precise value of m would require knowing all the channels down to zero frequency, i.e., an infinite wavelength, which is obviously not possible (Fig. 7). Notice that m is on the order of 10^4 for 30 m of PM fiber. As said very early by Rashleigh [2], channeled spectrum analysis is *inherently* a group measurement!

Notice finally that there is a *dual* technique to measure a channeled spectrum: *path-matched white light interferometry*. As it is well-known, the interference power P, as a function of the path unbalance ΔL_r of an interferometer, is the Fourier transform (FT) of the power spectrum of the input light. With the channeled spectrum created by the PM fiber under test, it yields a central peak with the fringe amplitude following the coherence function of the original broadband source, and also two symmetrical secondary peaks with a contrast C of 0.5, for $\Delta L_r = \pm B_g \cdot L_f$ (Fig. 8). This technique was developed to make a distributed measurement of polarization crossed couplings along a PM fiber [14–18].

4 Measurement techniques of phase birefringence *B*

The first techniques to measure phase birefringence were based on creating a localized crossed polarization coupling in the PM fiber with the magneto-optic Faraday effect [19], or with the application of a transverse force that creates additional stresses in the fiber, which modifies the orientation of the principal birefringence axes [20–23]. The set-ups that were used are quite complicated, but they all rely on the same basic idea: when the localized crossed coupling is moved along the fiber, it yields a modulation of the processed signal that has a period equal to the beat length Λ, that is simply related to phase birefringence B with $\Lambda = \lambda/B$, as we saw in (6).

One can understand it easily by considering a single wavelength source, at λ_0, that is coupled along one of the principal axes of the PM fiber. A localized polarization crossed coupling is created, and there is an output polarizer at 45° of the principal axes (Fig. 9a). This yields a polarimeter and a channeled spectrum like what we just saw,

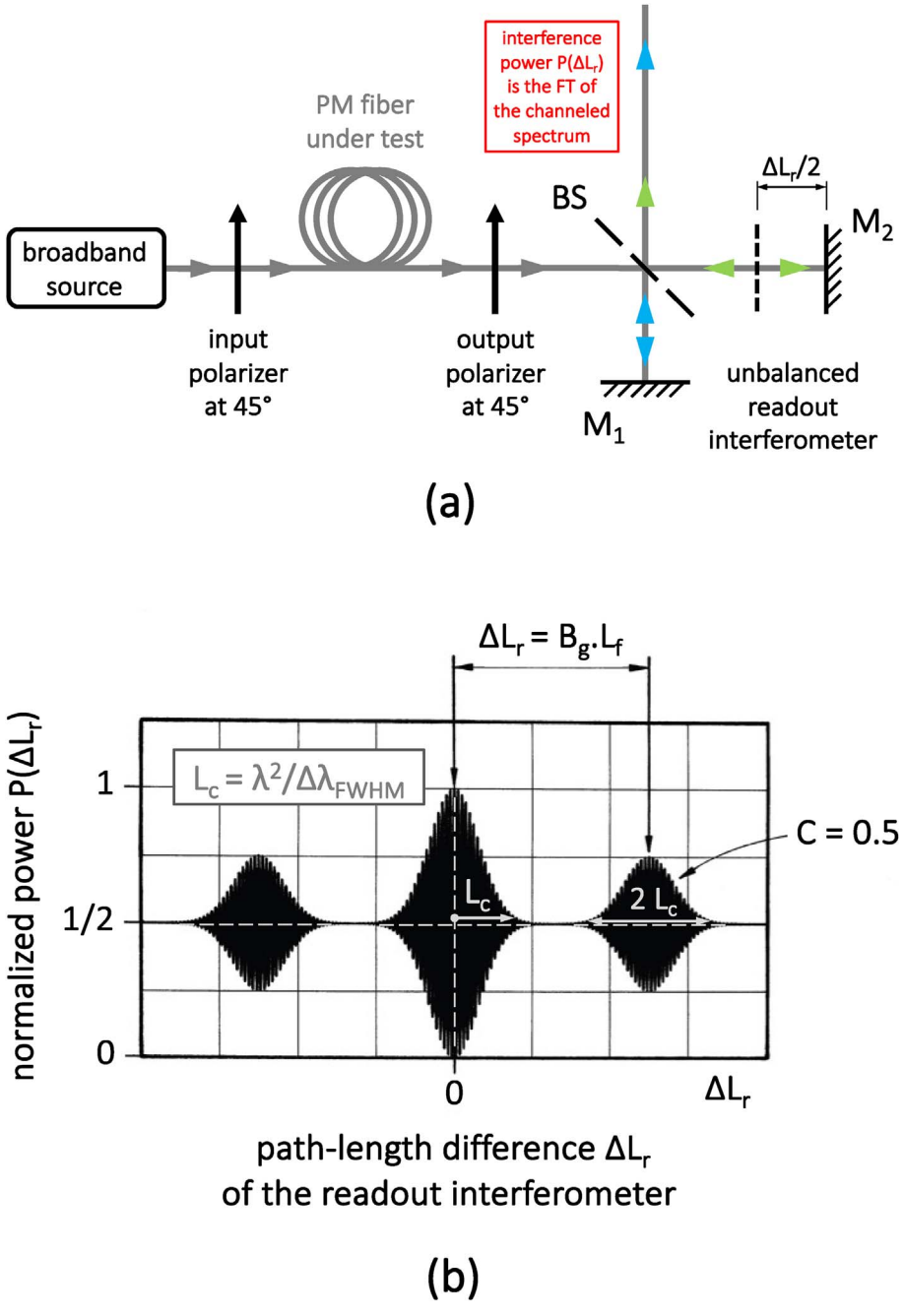

Figure 8. Principle of path-matched white-light interferometry: (a) set-up with an unbalanced readout interferometer, using a beam splitter BS, and two mirrors M_1 and M_2; (b) interferogram as a function of the path unbalance ΔL_r, with the secondary peaks yielding a measurement of group birefringence B_g; this interferogram is the Fourier transform (FT) of the channeled spectrum; and the coherence length L_c of the original broadband source is equal to $\lambda^2/\Delta\lambda_{\mathrm{FWHM}}$.

considering that the fiber length L_f is now the length between the localized coupling and the fiber end. The only difference is that the contrast is not perfect anymore since the crossed coupling is equivalent to a low reflectivity splitter. Assuming a power splitting ratio of ε^2 and $1-\varepsilon^2$, instead of 50–50, the contrast becomes 2ε. As well-known in interferometry, the contrast depends on the amplitude ratio ε between the two interfering waves, and not on the power ratio ε^2. It can be viewed simply, considering a main wave with a normalized amplitude of 1 and a low wave with a normalized amplitude of ε. Depending on their relative phase shift, the interference amplitude oscillates between $1+\varepsilon$ and $1-\varepsilon$; the interference power is then $(1\pm\varepsilon)^2 = 1\pm 2\varepsilon+\varepsilon^2 \approx 1\pm 2\varepsilon$.

As seen in (11), there is a bright channel when the length L_f between the coupling point and the PM fiber end yields an optical path length difference ΔL_{opt} equal to an integer number m of wavelength λ_0:

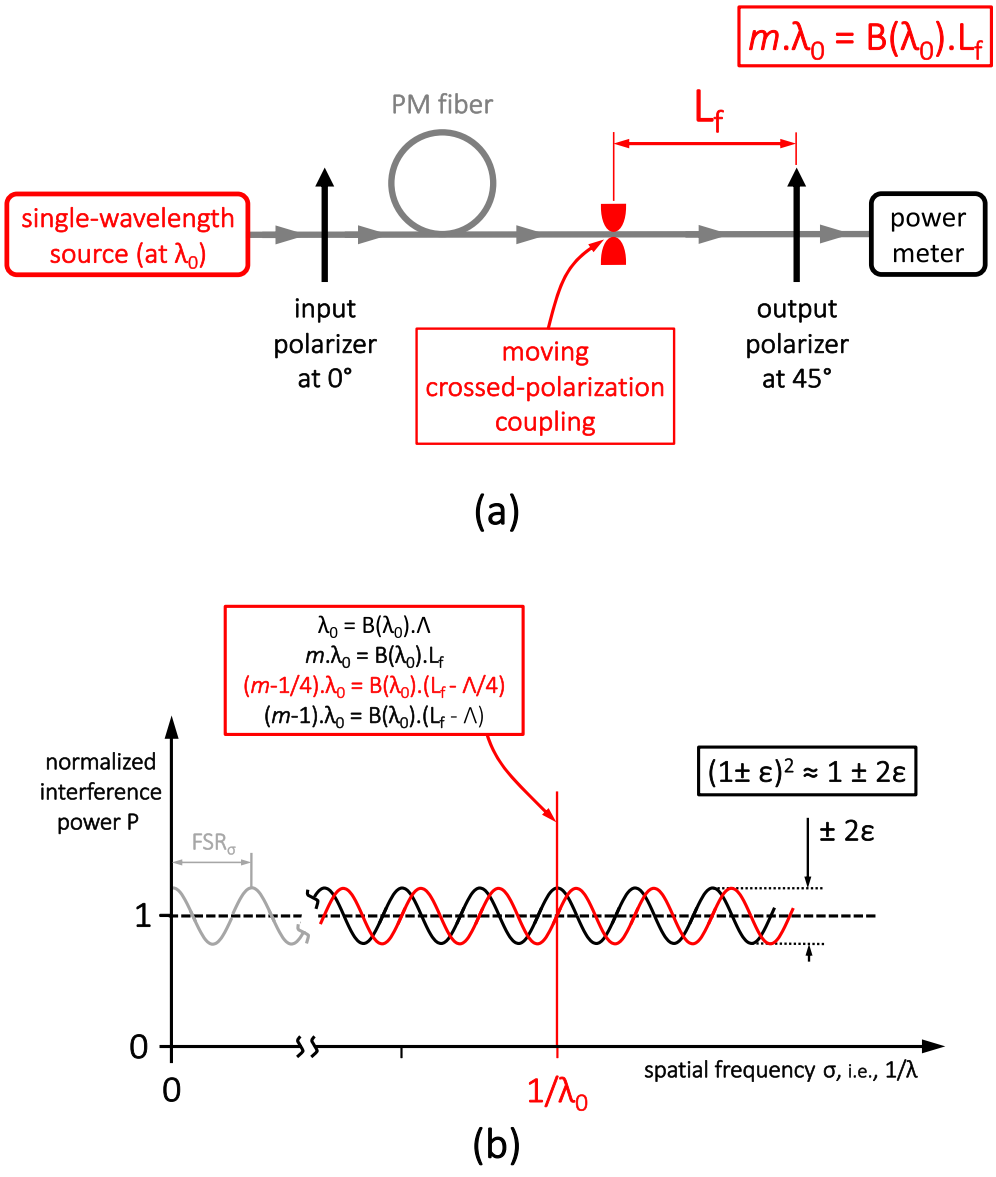

Figure 9. Measurement of phase birefringence $B(\lambda_0)$ of a PM fiber: (a) set-up with a moving crossed-polarization coupling; (b) resulting channeled spectrum (black sinusoidal curve) for a length L_f corresponding to a bright channel of order m for λ_0; and shifted channeled spectrum (red sinusoidal curve) when the length is reduced by a quarter of the beat length Λ, i.e., is equal to $L_f - (\Lambda/4)$.

$$\Delta L_{\text{opt}} = B(\lambda_0) \cdot L_f = m \cdot \lambda_0. \tag{20}$$

If this length L_f is reduced by a quarter of a beat length Λ, the channeled spectrum becomes shifted by a quarter of the fringe period since $B(\lambda_0) \cdot \Lambda = \lambda_0$, which reduces the output power. For half the beat length, the shift is half the period, and the power becomes minimum; for a full beat length, it is back to the maximum, but the channel order is then $m - 1$:

$$B(\lambda_0) \cdot \big(L_f - \Lambda\big) = (m-1) \cdot \lambda_0. \tag{21}$$

As we saw, channeled spectrum analysis does not allow one to get the precise value m of the channel order, but it is possible to know its *relative* variation by moving the crossed polarization coupling, which yields a measurement of the beat length Λ, and then of the *phase* birefringence $B(\lambda_0)$.

Another technique of phase birefringence measurement is the use of a fiber Bragg grating (FBG) [24], with a very low reflectivity to ensure that it does not modify the birefringence. The reflected wavelength λ_R is given by:

$$\lambda_R = 2n_{\text{eff}} \cdot \Lambda_{\text{Bragg}}, \tag{22}$$

where n_{eff} is the effective index of the fiber mode and Λ_{Bragg} is the period of the Bragg grating. A PM fiber being birefringent by principle, it yields two reflected

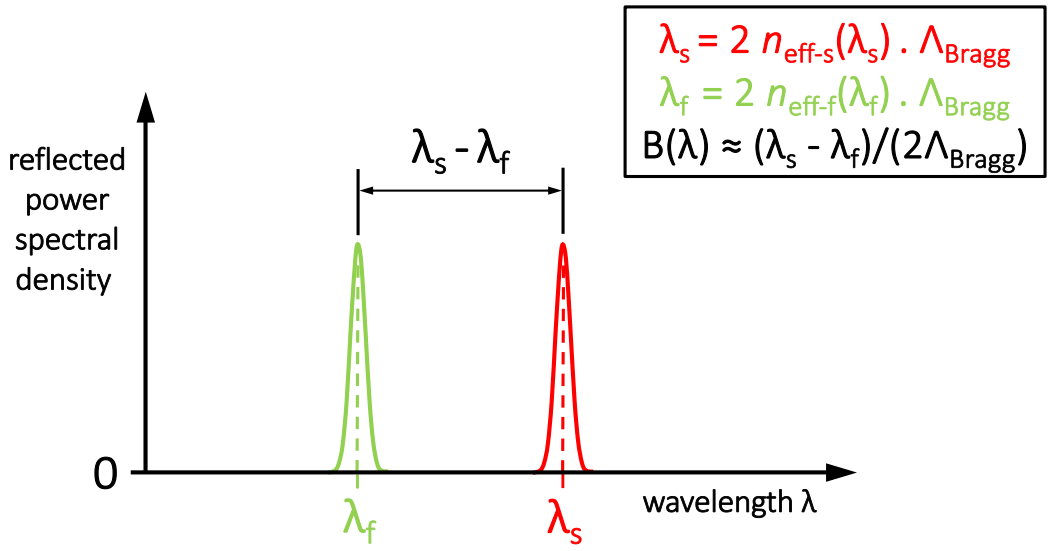

Figure 10. Measurement of phase birefringence $B(\lambda)$ of a PM fiber with a fiber Bragg grating that has a period Λ_{Bragg}; λ_f is the reflected wavelength of the fast (lower-index) mode, while λ_s is the one of the slow (higher-index) mode.

wavelengths, λ_s and λ_f, that correspond respectively to the effective index $n_{\text{eff}-\text{s}}$ of the slow mode, and $n_{\text{eff}-\text{f}}$, the one of the fast mode (Fig. 10), with:

$$\lambda_s = 2n_{\text{eff}-\text{s}}(\lambda_s) \cdot \Lambda_{\text{Bragg}} \text{ and } \lambda_f = 2n_{\text{eff}-\text{f}}(\lambda_f) \cdot \Lambda_{\text{Bragg}}. \quad (23)$$

The phase birefringence B is:

$$B(\lambda_f) = n_{\text{eff}-\text{s}}(\lambda_f) - n_{\text{eff}-\text{f}}(\lambda_f) \text{ or}$$
$$B(\lambda_s) = n_{\text{eff}-\text{s}}(\lambda_s) - n_{\text{eff}-\text{f}}(\lambda_s). \quad (24)$$

There are:

$$n_{\text{eff}-\text{s}}(\lambda_f) = n_{\text{eff}-\text{s}}(\lambda_s) + [(\lambda_f - \lambda_s) \cdot (\text{d}n_{\text{eff}-\text{s}}/\text{d}\lambda)] \text{ and}$$
$$n_{\text{eff}-\text{f}}(\lambda_s) = n_{\text{eff}-\text{f}}(\lambda_f) + [(\lambda_s - \lambda_f) \cdot (\text{d}n_{\text{eff}-\text{f}}/\text{d}\lambda)]. \quad (25)$$

Assuming that $\text{d}n_{\text{eff}-\text{s}}/\text{d}\lambda \approx \text{d}n_{\text{eff}-\text{f}}/\text{d}\lambda \approx \text{d}n_{\text{eff}}/\text{d}\lambda$, it yields:

$$B(\lambda_f) \approx B(\lambda_s) \approx (\lambda_s - \lambda_f) \cdot [(1/(2\Lambda_{\text{Bragg}})) - (\text{d}n_{\text{eff}}/\text{d}\lambda)]. \quad (26)$$

Phase dispersion $\text{d}n_{\text{SiO}_2}/\text{d}\lambda$ of silica is about -0.01 µm^{-1} in the 1200–1600 nm range [1], and waveguide phase dispersion is about -0.005 µm^{-1} for a single mode fiber with a numerical aperture NA of 0.19, i.e., a core index step of 0.0125 [1], whilst $1/(2\Lambda_{\text{Bragg}})$ is about 1 µm^{-1} at 1550 nm. Therefore, within an approximation of 1.5%, phase birefringence $B(\lambda)$ is simply:

$$B(\lambda) \approx (\lambda_s - \lambda_f)/(2\Lambda_{\text{Bragg}}). \quad (27)$$

A last method is based on Rayleigh-OFDR (Rayleigh optical-frequency-domain reflectometry). This technique developed by Froggatt and co-workers [25] is impressive, and a commercial test instrument is available (OBR 4600 by Luna). OFDR was proposed very early by Eickhoff and Ulrich [26]. They explained it in terms of radar specialists with frequency chirp, temporal delay, and frequency beating, but it can be also viewed as channeled spectrum analysis, which is much easier to understand for optics-photonics specialists.

It is like what we saw earlier in Figure 9. Instead of a polarimeter, it is a two-wave interferometer with a reference mirror on one arm and a small reflection (ε^2 in power) on the measurement arm. It yields a channeled spectrum that is measured with a tunable laser; the contrast is 2ε, and there are bright channels when the optical path length difference, $\Delta L_{\text{opt}} = 2n_{\text{eff}} \cdot \Delta L_f$, is equal to an integer number of wavelength λ. ΔL_f is the fiber length difference between the reference mirror and the low reflection, and n_{eff} is the effective index of the mode (Fig. 11).

As in (13) for the polarimeter, the mth channel follows $m = \Delta L_{\text{opt}} \cdot \sigma(m)$ and, for the interferometer, it yields:

$$m = 2n_{\text{eff}} \cdot \Delta L_f \cdot \sigma(m). \quad (28)$$

With a PM fiber, one can select the slow mode or the fast one, and there is:

$$m = 2n_{\text{eff}-\text{s}} \cdot \Delta L_f \cdot \sigma_s(m) = 2n_{\text{eff}-\text{f}} \cdot \Delta L_f \cdot \sigma_f(m). \quad (29)$$

There is a frequency shift $\Delta\sigma$ between the respective channeled spectra (Fig. 12a). The frequency of the mth channel of the slow mode is $\sigma_s(m)$, and it is $\sigma_f(m)$ for the fast mode. Since:

$$n_{\text{eff}-\text{s}} \cdot \sigma_s(m) = n_{\text{eff}-\text{f}} \cdot \sigma_f(m). \quad (30)$$

There is:

$$B = n_{\text{eff}-\text{s}} - n_{\text{eff}-\text{f}} = n_{\text{eff}-\text{f}} \cdot (\sigma_f - \sigma_s)/\sigma_s. \quad (31)$$

Considering the mean effective index n_{eff}, and the mean spatial frequency σ, it yields:

$$B \approx n_{\text{eff}} \cdot (\sigma_f - \sigma_s)/\sigma = n_{\text{eff}} \cdot \Delta\sigma/\sigma. \quad (32)$$

With (32), one could then think that it is possible to measure phase birefringence B, while we saw earlier

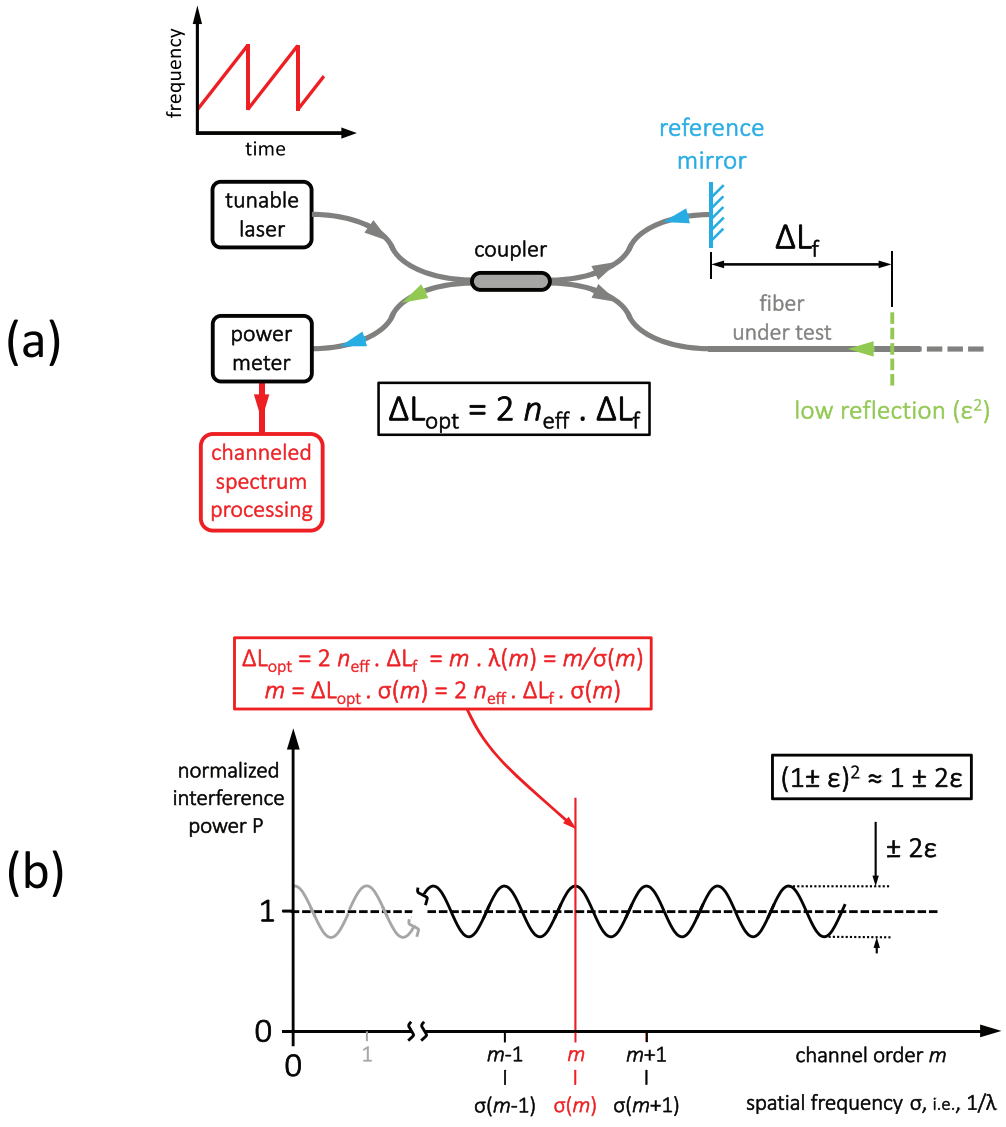

Figure 11. Principle of OFDR: (a) set-up with a frequency-swept tunable laser, an unbalanced two-wave interferometer with a reference mirror on one arm, and the low reflection point (ε^2 in power, and ε in amplitude) that is analyzed, on the other arm; (b) measured channeled spectrum with a contrast of 2ε.

that channeled spectrum analysis *inherently measures group delay and not phase delay* [2]. Actually, it is not possible because one can decide that a certain channel of the slow-mode spectrum is the mth one, but there is *no mean* to know where is the corresponding mth channel of the fast-mode spectrum: shifted sine functions *cannot be correlated* over more than one period (Fig. 12a).

The question is then why is it possible to measure phase birefringence B with Rayleigh-OFDR, as proposed by Froggatt and co-workers [25]? As seen in Section 2, Rayleigh scattering is based on dipolar antenna emission of the numerous covalent Si–O bonds of silica, that are excited by the E field of the incoming light. Silica has a glassy (or amorphous) structure, and these bonds are randomly positioned; they are equivalent to many low-reflection points randomly distributed along the fiber. With channeled-spectrum analysis, it yields a channeled spectrum that looks like a white noise, instead of the sine function obtained with a single reflector. Now, the randomness of the positions of these reflectors is fixed for a given fiber, and the Rayleigh channeled spectrum obtained with OFDR is an actual *signature of the fiber* [25]. Testing with the slow mode and the fast mode yields two identical *noisy* channeled spectra that are offset by the frequency shift $\Delta\sigma$ (Fig. 12b). This shift is identical to the first case with sine spectra but now, *noisy channeled spectra can be cross-correlated* to know $\Delta\sigma$, and then phase birefringence B, with (32), which is a great idea. However, this explanation is very simplified to allow the reader to grasp the principle of the method, but the signal processing of Rayleigh-OFDR is actually very sophisticated [25] … and impressive!

We saw in Sections 2 and 3 that channel spectrum analysis of birefringence can use three equivalent methods:

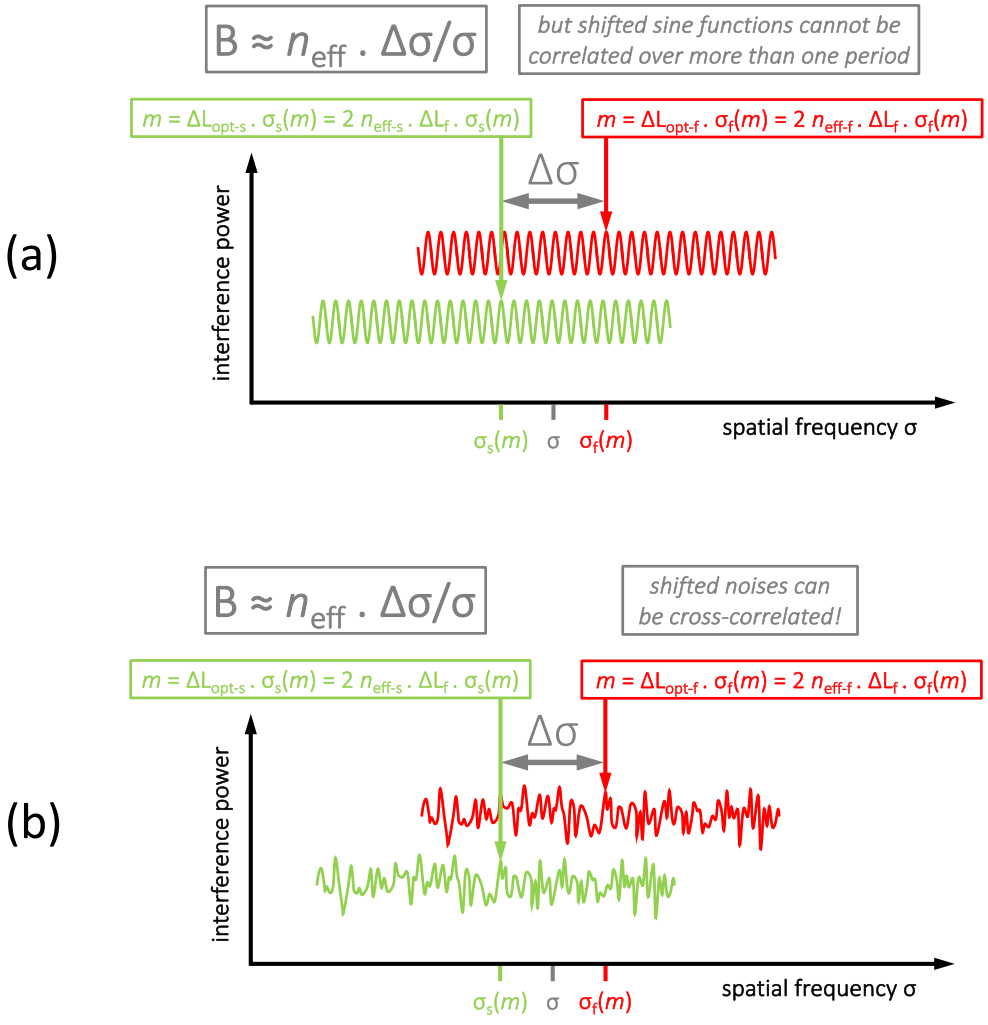

Figure 12. Shifted channeled spectra, using the slow mode (green curves) and the fast mode (red curves) of a PM fiber: (a) case of a single reflector with sine spectra that *cannot* be correlated over more than one period; (b) case of Rayleigh backscattering with noisy spectra that *can* be cross-correlated.

broadband source with an OSA, tunable laser, or path-matched white-light interferometry. It is the same for reflectometry but, if the three methods are equivalent, they do not have at all the same noise floor to detect very low reflections. With an OSA, the simplest technique, it is only −70 dB, which corresponds to a back-reflection of 3×10^{-4} in amplitude, and 10^{-7} in power; with path-matched white light interferometry, it is typically −90/−100 dB; with a tunable laser, as used in OFDR, it can go down to −130 dB [18]. Rayleigh backscattering signal is around −110 dB, and it requires OFDR to be measurable.

These three equivalent methods do not have at all the same spectral resolution either. For an OSA (Fig. 2), it is typically $\Delta\lambda_{\mathrm{OSA}} \approx 0.01$ nm. The free spectral range in spatial frequency, FSR_σ, is $1/\Delta L_{\mathrm{opt-g}}$, where $\Delta L_{\mathrm{opt-g}}$ is the group optical path length difference, i.e., $(n_g/n) \cdot \Delta L_{\mathrm{opt}}$. In wavelength, it is:

$$\mathrm{FSR}_\lambda = \frac{\lambda^2}{\Delta L_{\mathrm{opt-g}}}. \tag{33}$$

Then, the maximum path length, $\Delta L_{\max}$, that can be explored is:

$$\Delta L_{\max} = \lambda^2/\Delta\lambda_{\mathrm{OSA}}. \tag{34}$$

For $\Delta\lambda_{\mathrm{OSA}} = 0.01$ nm at 1550 nm, $\Delta L_{\max}$ is about 25 cm; it means about 8 cm of fiber in reflectometry, where $n_g \approx 1.45$, and about 500 m in a polarimeter, where $B_g \approx 5 \times 10^{-4}$.

With path-matched interferometry, it depends on the travel distance of the moving mirror M_2 of the read-out interferometer (Fig. 8). In practice, it is difficult to have more than few meters, even with a multi-fold path. With a tunable laser that has a very narrow linewidth, it yields a great spectral resolution, and the maximum path length,

$\Delta L_{\max}$, can go up to few kilometers, as seen with the OBR 4600 of Luna. Impressive!

5 How to derive phase birefringence $B(\lambda)$ from group birefringence $B_g(\lambda)$

As we saw, measurement of group birefringence $B_g(\lambda)$ over a wide spectrum is very easy with channeled spectrum analysis using a broadband source and an OSA, while measurement of phase birefringence B is more complicated, even if it is not too difficult for a single wavelength. Reference [1] presented a geometrical construction to derive group birefringence $B_g(\lambda)$ from phase birefringence $B(\lambda)$, while one has now to derive $B(\lambda)$ from $B_g(\lambda)$ and a single measurement $B(\lambda_0)$.

As seen in [1], group birefringence $B_g(\lambda)$ is related to phase birefringence $B(\lambda)$ with:

$$B_g(\lambda) = B(\lambda) - [\lambda \cdot B'(\lambda)]. \tag{35}$$

And the tangent $T_i(\lambda)$ to the curve $B(\lambda)$, at the wavelength λ_i, follows:

$$T_i(\lambda) = B(\lambda_i) + [(\lambda - \lambda_i) \cdot B'(\lambda_i)]. \tag{36}$$

Then:

$$T_i(0) = B(\lambda_i) - [(\lambda_i) \cdot B'(\lambda_i)] = B_g(\lambda_i). \tag{37}$$

Knowing phase birefringence $B(\lambda)$ and its derivative $B'(\lambda)$, over a wide spectrum, allows one to retrieve group birefringence $B_g(\lambda)$ over this wide spectrum with a simple geometrical construction, using the tangent to $B(\lambda)$ (Fig. 13).

Conversely, if one knows the whole curve $B_g(\lambda)$ and a single value $B(\lambda_1)$ for phase birefringence, one can define the tangent $T_1(\lambda)$ and the derivative $B'(\lambda_1)$. However, one cannot define *yet* the tangent $T_2(\lambda)$, nor $B(\lambda_2)$, for another wavelength λ_2. One must do some math to get it.

We saw in (35) that $B_g(\lambda) = B(\lambda) - [\lambda \cdot B'(\lambda)]$. It yields for the derivatives:

$$B_g^{'}(\lambda) = -\lambda \cdot B''(\lambda) \text{ and } B''(\lambda) = -B_g^{'}(\lambda)/\lambda \tag{38}$$

and there is also:

$$B(\lambda) = B_g(\mathrm{d}\lambda) + [\lambda \cdot B'(\lambda)]. \tag{39}$$

One can integrate $B^{''}(\lambda)$, seen in (38), to get $B'(\lambda)$:

$$B'(\lambda_2) = B'(\lambda_1) - \int_{\lambda_1}^{\lambda_2} (B_g'(\lambda)/\lambda) \cdot \mathrm{d}\lambda \tag{40}$$

and phase birefringence $B(\lambda)$ for λ_2 can be retrieved:

$$B(\lambda_2) = B_g(\lambda_2) + [\lambda_2 \cdot B'(\lambda_1)] - \left[\lambda_2 \cdot \int_{\lambda_1}^{\lambda_2} \left(\frac{B_g'(\lambda)}{\lambda}\right) \cdot \mathrm{d}\lambda\right]. \tag{41}$$

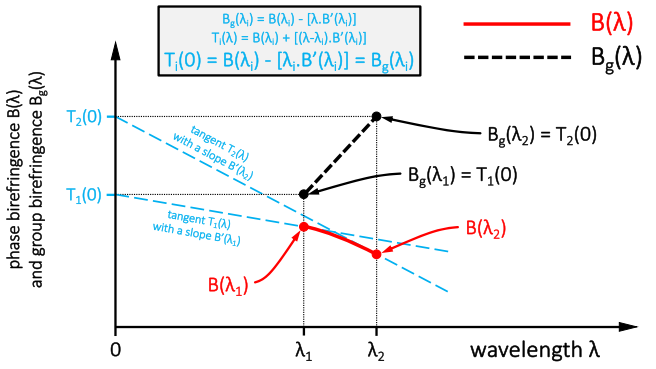

Figure 13. Geometrical construction to derive group birefringence $B_g(\lambda)$ (dashed black curve) from phase birefringence $B(\lambda)$ (red solid curve), as seen in [1]; the tangents $T_i(\lambda)$ (blue dashed lines) cross the ordinate axis, i.e., where $\lambda = 0$, at $B_g(\lambda_i)$; cases with $i = 1$ or 2.

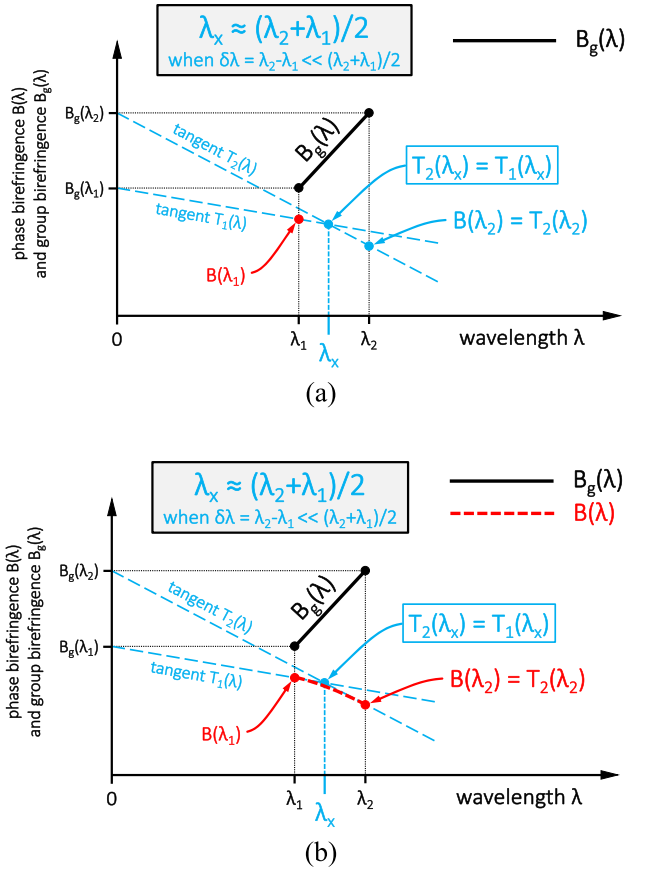

Figure 14. Geometrical construction to derive phase birefringence $B(\lambda)$ from group birefringence $B_g(\lambda)$ (black solid line) and a single-wavelength phase measurement $B(\lambda_1)$ (red circular dot); (a) construction of the tangent $T_2(\lambda)$ that crosses tangent $T_1(\lambda)$ at $\lambda_x = (\lambda_2 - \lambda_1)/\ln(\lambda_2/\lambda_1)$ (dashed blue lines), which allows one to find $B(\lambda_2)$;when the interval $(\lambda_2 - \lambda_1)/\lambda_1$ is small, $\lambda_x \approx (\lambda_2 + \lambda_1)/2$; (b) construction of $B(\lambda)$ (dashed red curve) that must fit the tangents $T_1(\lambda)$ and $T_2(\lambda)$.

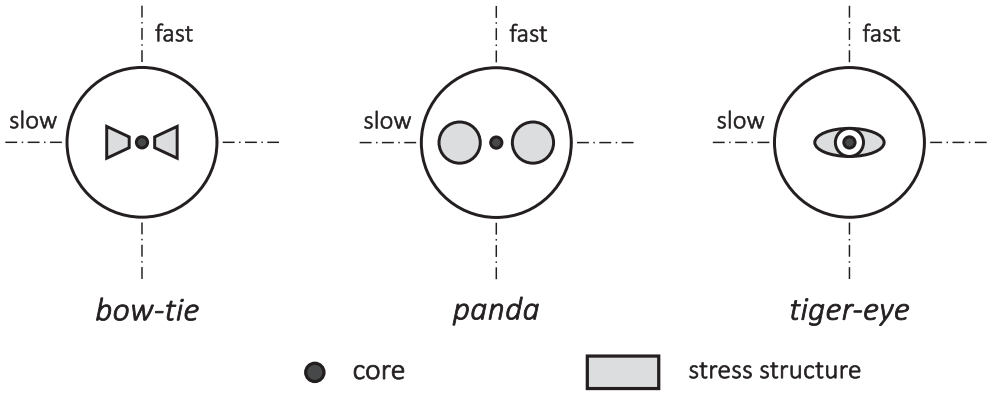

Figure 15. Different kinds of PM fibers based on stress-induced linear birefringence: bow-tie, panda and tiger-eye. The slow axis is along the axis of the stress structure, and the fast axis is perpendicular.

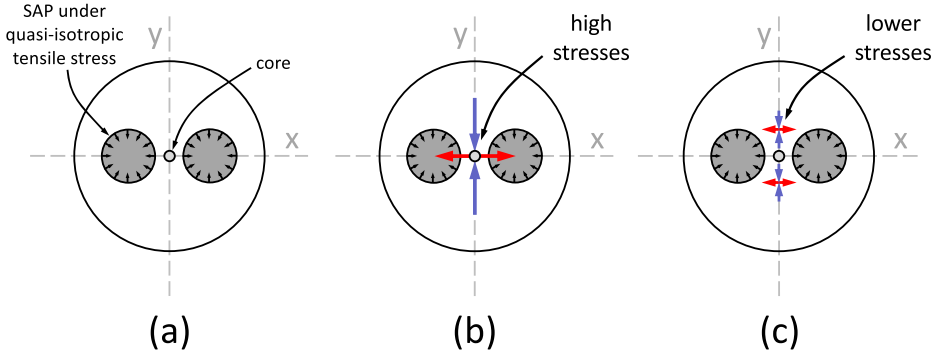

Figure 16. Principle of PM fibers based on stress-induced linear birefringence: (a) SAPs (panda structure, here) are under quasi-isotropic tensile stress, and they pull on the fiber cladding; (b) in the core region, this yields tensile stress (red arrows) in the x-axis, and a compressive stress (blue arrows) in the perpendicular y-axis; (c) these stresses decrease when one moves away from the core, along the perpendicular y-axis.

With a small interval between λ_1 and λ_2, one can consider that the slope B'_g of $B_g(\lambda)$ is constant and:

$$B(\lambda_2) = B_g(\lambda_2) + [\lambda_2 \cdot B'(\lambda_1)] - \left[\lambda_2 \cdot B'_g \cdot \int_{\lambda_1}^{\lambda_2} \frac{\mathrm{d}\lambda}{\lambda}\right], \quad (42)$$

$$B(\lambda_2) = B_g(\lambda_2) + [\lambda_2 \cdot B'(\lambda_1)] - [\lambda_2 \cdot B'_g \cdot \ln(\lambda_2/\lambda_1)]. \quad (43)$$

A geometrical construction remains possible, using again the tangents $T_i(\lambda)$. Equations (36) and (37) yield:

$$T_i(\lambda) = B_g(\lambda_i) + [\lambda \cdot B'(\lambda_i)]. \quad (44)$$

They cross each other for the wavelength λ_x where $T_1(\lambda_x) = T_2(\lambda_x)$, and then:

$$\lambda_x = -[B_g(\lambda_2) - B_g(\lambda_1)]/[B'(\lambda_2) - B'(\lambda_1)]. \quad (45)$$

There is $B_g(\lambda_2) - B_g(\lambda_1) \approx B'_g \cdot (\lambda_2 - \lambda_1)$ and, from (40):

$$B'(\lambda_2) - B'(\lambda_1) \approx -B'_g \cdot \int_{\lambda_1}^{\lambda_2} \frac{\mathrm{d}\lambda}{\lambda} = -B'_g \cdot \ln(\lambda_2/\lambda_1). \quad (46)$$

It yields:

$$\lambda_x = (\lambda_2 - \lambda_1)/\ln(\lambda_2/\lambda_1). \quad (47)$$

The Taylor series of natural logarithm, ln, leads to:

$$\ln(1+\delta) = \delta - \delta^2/2 + \delta^3/3 - \delta^4/4 + \cdots \quad (48)$$

Therefore, when the interval $\delta = (\lambda_2 - \lambda_1)/\lambda_1$ is small, there is:

$$\lambda_x \approx \lambda_1(1 + \delta/2) = (\lambda_2 + \lambda_1)/2. \quad (49)$$

The wavelength λ_x is simply in the middle of the interval between λ_1 and λ_2, which makes the geometrical construction easy (Fig. 14). We know $B_g(\lambda)$ and $B(\lambda_1)$; we can deduce $T_1(\lambda)$ with $B_g(\lambda_1)$ and $B(\lambda_1)$; we can find $T_2(\lambda)$ with $B_g(\lambda_2)$, and also $T_2(\lambda_x) = T_1(\lambda_x)$, with $\lambda_x \approx (\lambda_2 + \lambda_1)/2$; finally, we can construct the curve $B(\lambda)$ between λ_1 and λ_2, with the two tangents $T_2(\lambda)$ and $T_1(\lambda)$.

6 Origin of birefringence dispersion in PM fibers using stress-induced birefringence

The method, that is now widely generalized to make PM fibers, is to use stress-induced linear birefringence with

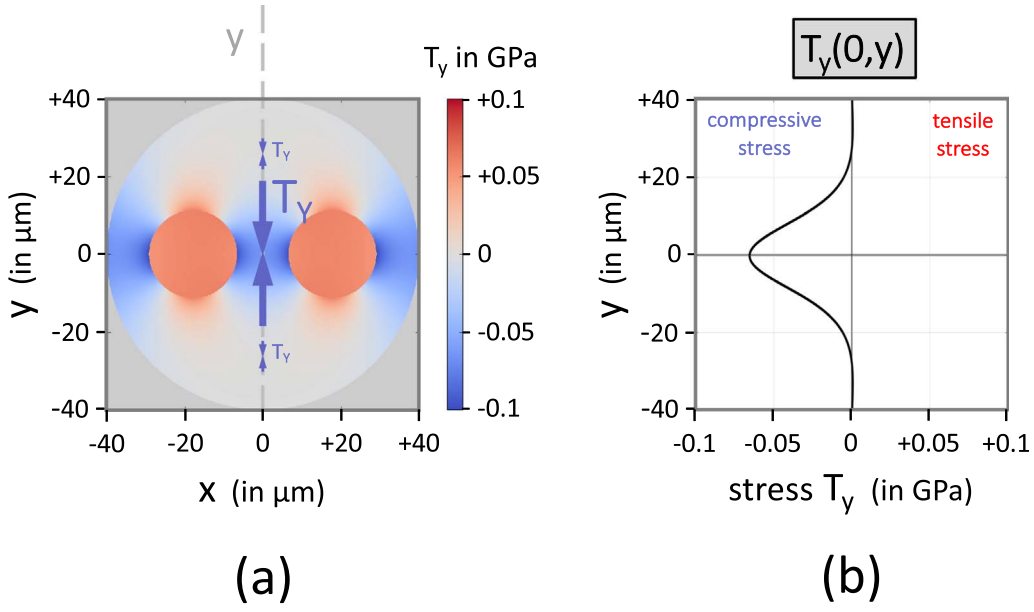

Figure 17. Numerical model of the compressive stress $T_y(x,y)$, in a panda fiber, *without the circular core*, not to be *blinded* by the significant *isotropic* stress that this one generates: (a) color code with, in addition, double arrows to better visualize the stresses; (b) curve $T_y(0,y)$ of the compressive stress in the y-axis that decreases along this y-axis, and gets to zero at the outer limit of the cladding.

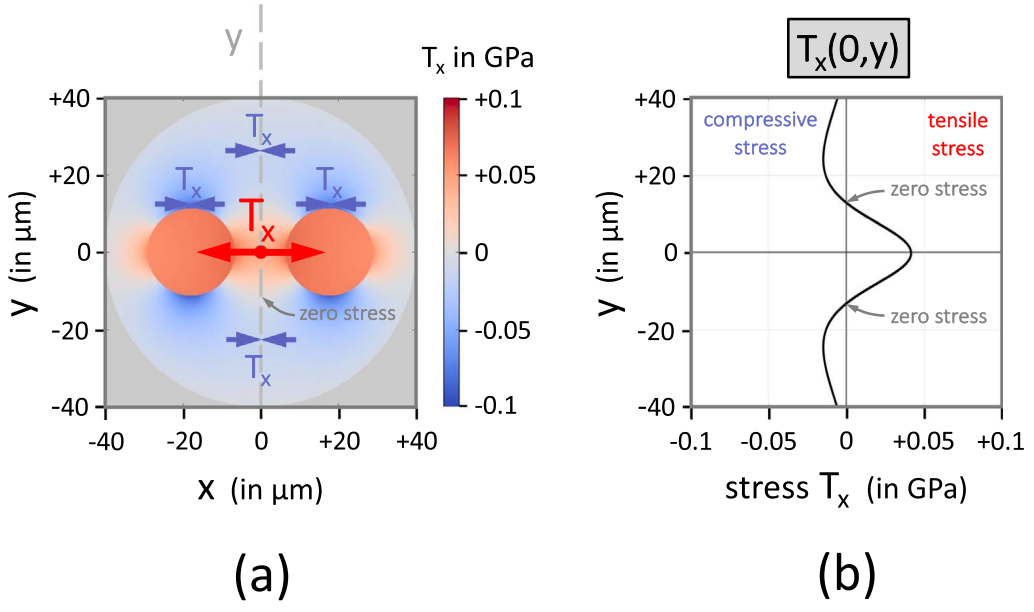

Figure 18. Numerical model of the stress $T_x(x,y)$ in a panda fiber, *without the circular core*, not to be *blinded* by the significant *isotropic* stress that this one generates: (a) color code with, in addition, double arrows to better visualize the stresses; (b) curve $T_x(0,y)$ of the variation of the stress on the x-axis, along the y-axis: it is positive in the core region, and it becomes negative at a distance that corresponds to about the height of the SAPs.

additional materials that have a thermal expansion coefficient larger than silica (several 10^{-6}/°C instead of 5×10^{-7}/°C for pure silica). The fiber preform is fabricated with two rods (sometimes called stress-applying parts, or SAPs) of highly doped silica (usually with boron and/or phosphorous) located on each side of the core region. Present PM products are based on three techniques that lead to similar results, as we shall see in the next section. They have *nicknames* based on obvious similarities with their look: *bow-tie*, *panda* and *tiger-eye* (Fig. 15). After pulling the fiber at high temperature, these highly doped rods will tend to contract on cooling, but their thermal contraction is blocked by the surrounding silica, which has a much lower thermal contraction. This puts the rods under

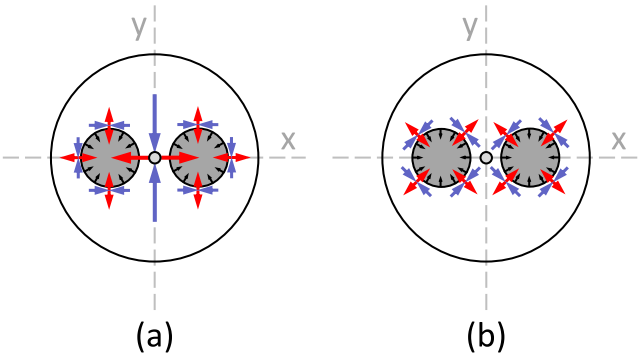

Figure 19. Stresses around the SAPs: (a) at 0° and 90°; (b) at 45°, where the sum of their projections on the x or y-axis becomes null ... but it does not mean that the stresses are null!

quasi-isotropic tensile stress, and, by reaction, this also induces stresses in the core region where light propagates; there is a tensile stress in the x-axis of the rods and a compressive stress in the perpendicular y-axis. Because of the photo-elastic effect, these anisotropic stresses yield anisotropic index changes, i.e., birefringence. These stresses are quite uniform along the x-axis between the rods (or SAPs), but they decrease rapidly along the perpendicular y-axis (Fig. 16). This creates birefringence dispersion since a longer wavelength yields a wider mode that sees lower stresses, which reduces the birefringence. The derivative $B'(\lambda)$ of phase birefringence $B(\lambda)$ is negative, and then, group birefringence $B_g(\lambda)$ is larger than $B(\lambda)$, since $B_g(\lambda) = B(\lambda) - [\lambda \cdot B'(\lambda)]$, as seen in (35).

We made a numerical model that confirms this behavior. In this model, we *do not* include the circular core to avoid being *blinded* by the significant isotropic stress that this one generates. Because of the high thermal expansion of germania (GeO_2) glass, the germano-silicate core behaves like the SAPs, but the additional isotropic stress that is created does not give any birefringence. To suppress the core in the model is easing the understanding: we clearly see that the compressive stress $T_y(x,y)$ does decrease, in absolute value, along the y-axis to get to zero at the outer surface of the cladding (Fig. 17).

The stress $T_x(x,y)$ on the x-axis does also decrease along the y-axis; this is even faster than for $T_y(0,y)$. The curve $T_x(0,y)$ is positive (tensile stress) in the core region, becomes null and gets negative (compressive stress) (Fig. 18).

Note that the color code produces an *artefact*: when the stresses are at 45° of the axes, the color corresponds to the sum of the projections on these axes. Around the SAPs, the orthogonal stress is positive (tensile), while the tangential stress is negative (compressive); they have about the same absolute value and, at 45°, the *sum of their projections* on the x or y axes becomes null ... but it does not mean that the stresses are null (Fig. 19)!

There is a second source of birefringence dispersion that *is not often mentioned*: dispersion of the photo-elastic effect in silica. This effect is usually treated with two photo-elastic coefficients: p_{11} and p_{12} that are dimensionless since they are related to elastic strains that are also dimensionless. They are assumed to be wavelength independent in most

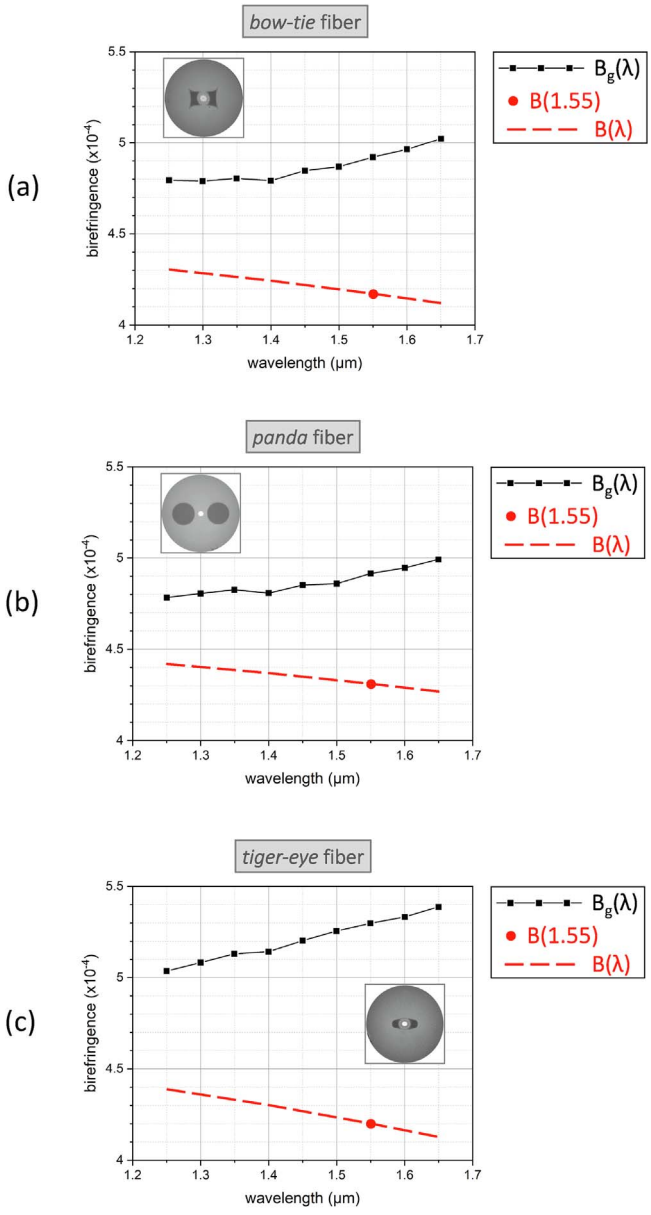

Figure 20. Measured group birefringence $B_g(\lambda)$ over 1250–1650 nm (black solid line, with square dots for the measurements), measured phase birefringence B at 1550 nm (red circular dot), and deduced phase birefringence $B(\lambda)$ over 1250–1650 nm (red dashed line): (a) bow-tie fiber; (b) panda fiber; (c) tiger-eye fiber. Photographs of the end face of the fibers are inserted; SAPs are dark, while the circular cores are illuminated.

publications, with $p_{11} = 0.121$ and $p_{12} = 0.270$. *To be honest*, it is what we had in mind!

It is Rashleigh ... *again* ... who outlined in his *great* 1983 letter [2] that it is not completely negligible. In his references, he cited a publication of Sinha [27] about this dispersive effect in bulk silica. With Figure 4 of this Sinha's paper, one can estimate that the *relative* variation of the photo-elastic effect is about *minus* 0.05 μm^{-1} in the 1.2–1.6 μm range. Applying this on the geometrical construction that relates group birefringence to phase birefringence

(Fig. 13), it yields a difference of 8% between them, at 1550 nm. The *very interesting result* of Sinha's paper is that the relative dispersion of the photo-elastic effect in silica, i.e., *fused* quartz, follows the same law as the relative dispersion of birefringence in *crystallin* quartz!

A similar relative variation of $-0.05\ \mu m^{-1}$ can be evaluated with Figure 6 of reference [28], that also cites Sinha [27]. Note that the title of this last reference of 1983 used *modal birefringence* for what is called phase birefringence today, and *polarization mode dispersion* (PMD) for what is called group birefringence, as outlined in Section 5 of [1]. There is the same use of vocabulary in reference [22] of 1993. We prefer to save the term PMD for *coupled-mode* PMD in low-birefringence telecom fibers, where it is a random process that grows as the square root of the length [29]. With high-birefringence PM fibers, it is actually *intrinsic* PMD that grows linearly with the fiber length. In this case, the concept of group birefringence looks more convenient to us [1].

7 Measurement of birefringence dispersion in PM fibers that use stress- induced birefringence.

We performed measurements of birefringence of the three standard kinds of PM fibers based on stress-induced birefringence: bow-tie, panda and tiger-eye (Fig. 15). Group birefringence B_g was measured with channeled spectrum analysis over a very wide spectrum (1250–1650 nm), using an in-house *supercontinuum* fiber source and an OSA (Fig. 2). The three fibers have about the same characteristics: cut-off wavelength λ_c around 1250–1350 nm for an operating wavelength of 1550 nm, numerical aperture (NA) of 0.19, i.e., core index step of 0.0125, mode-field diameter at $1/e$ (MFD) of 7 μm, and cladding diameter of 80 μm. Phase birefringence B was measured at 1550 nm with a Bragg grating, and also with Rayleigh-OFDR (OBR 4600 of Luna), with similar results. B was then deduced over the 1250–1650 nm range with the geometrical construction of Figure 14.

Results presented in Figure 20 show that the three fibers have similar phase birefringence $B(\lambda)$: around 4.2×10^{-4}; it corresponds to a beat length Λ of about 3.7 mm @ 1550 nm. As we already saw, the *historical habit* is to give the beat length @ 633 nm in commercial product specification sheets, but it is just *calculated* with the ratio of the wavelengths, which would yield here $3.7 \times (633/1550) \approx 1.5$ mm. Because of birefringence dispersion, it is clear that this habit should be abandoned, or at least explained.

From (35), one sees that the slope of the *relative* variation of the phase birefringence $B(\lambda)$ is:

$$B'/B = [1-(B_g/B)]/\lambda. \tag{50}$$

At 1550 nm, it is $-0.11\ \mu m^{-1}$ for the bow-tie fiber, $-0.09\ \mu m^{-1}$ for the panda fiber, and $-0.17\ \mu m^{-1}$ for the tiger-eye fiber, when the sole relative dispersion of the photo-elastic effect is $-0.05\ \mu m^{-1}$, as we just saw. The breakdown between the dispersion due to the decay of the stresses, away from the core, and the pure photo-elastic dispersion is about half and half for the bow-tie and panda fibers, and it is about two thirds-one third for the tiger-eye fiber. This last higher value is due to the smaller height of the SAPs of the tiger-eye fiber, which yields a faster decay of the stresses, away from the core.

The three fibers have also a significant dispersion of group birefringence, with a relative variation B'_g/B_g of about $+0.16\ \mu m^{-1}$, at 1550 nm. This must be considered with distributed measurement of polarization crossed couplings along a PM fiber [17, 18].

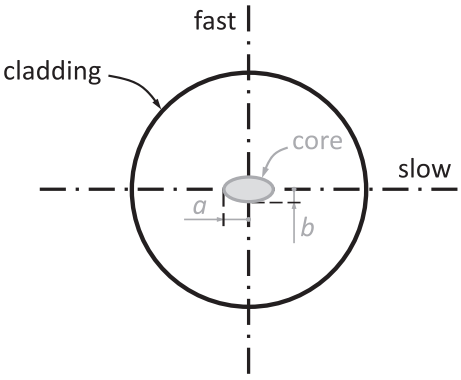

Figure 21. Elliptical-core (E-core) PM fiber, based on shape birefringence, with its slow and fast axes.

8 Case of an elliptical-core (E-core) PM fiber

The case of an elliptical-core, or *E-core*, PM fiber (Fig. 21) is much more complicated. There is *shape* birefringence induced by the elliptical core, but also stress-induced birefringence, and both are very dispersive. For shape birefringence, it involves difficult math. There are many publications on the subject, but, for us, the *less* complicated one is by Kumar and Ghatak [30] ... even if they must solve two *simple transcendental* equations ... which can be viewed as an *oxymoron*! A first simple important result is that shape phase birefringence depends on the square of the index step Δn of the core: this requires a high-index step to get enough birefringence, which implies a very small core to remain single mode. The other simple important result is that this shape birefringence saturates when the ratio between the major-axis width, $2a$, and the minor-axis one, $2b$, becomes higher than 2: it reaches the birefringence of a planar waveguide that has a thickness of $2b$.

This calls for a comment: the origin of shape birefringence can be grasped simply. As well-known, or at least known, in bulk optics, there is a phase shift with total internal reflection (TIR) and it depends on the state of polarization, s (perpendicular to the plane of incidence; s comes from *senkrech*, i.e., perpendicular in German), or p (parallel to the plane of incidence) (Fig. 22). These states correspond respectively to the TE (transverse electric) mode or the TM (transverse magnetic) mode of a planar waveguide. Shape birefringence is, for us, simply due to this difference of phase shift. It is the opportunity to recall that TIR phase shift

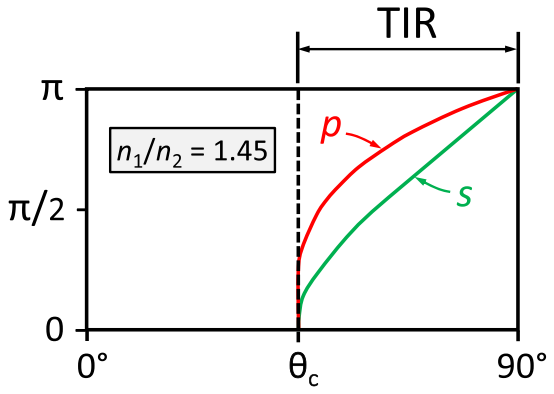

Figure 22. Phase shift induced by total internal reflection (TIR): p state of polarization is in red line, and s state is in green line. θ_c is the critical angle where TIR starts. A grazing incidence (angle of 90°) yields a π phase shift.

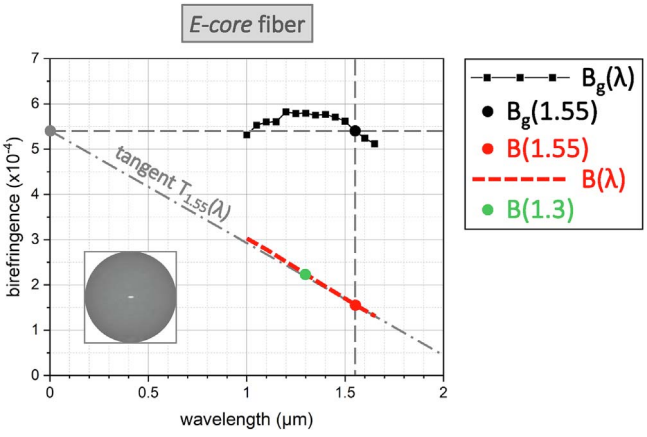

Figure 23. Measurement, by channeled spectrum analysis, of group birefringence $B_g(\lambda)$ of an E-core fiber, over 1000–1650 nm (black square dots); measurement of phase birefringence B at 1550 nm with Bragg grating and Rayleigh-OFDR (red circular dot); phase birefringence $B(\lambda)$ over 1000–1650 nm (dash red line) deduced by geometrical construction; confirmation of the value of B at 1300 nm with an additional Bragg grating (green circular dot); a photograph of the end face of the fiber, with its illuminated elliptical core, is inserted.

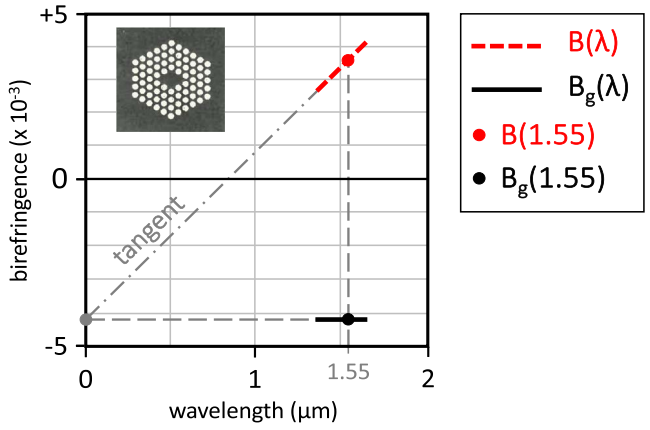

Figure 24. *Revisited* Figure 3 of [32]: the phase-birefringence dispersion $\mathrm{d}B/\mathrm{d}\lambda$ is very high, and it has a positive slope; this yields a group birefringence B_g with an opposite sign. This figure shows the interest of the geometrical construction with the tangent, that allows one to visualize simply the relationship between phase and group birefringences. The insert shows the shape of the micro-structured solid-core PM fiber described in [32].

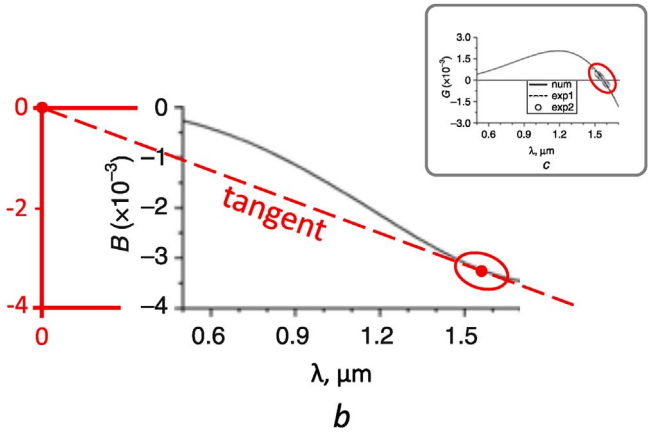

Figure 25. *Revisited* Figure 3b of [33]: the tangent to phase birefringence curve $B(\lambda)$ does cross at zero the *zero-wavelength* ordinate axis, for 1.55 μm, where group birefringence is cancelled; the insert shows Figure 3c, with group birefringence curve $B_g(\lambda)$, noted as $G(\lambda)$, in this paper.

difference is the principle of the Fresnel rhomb that gives a quarter-wave retarder. It is a very *broadband* retarder since the retardation depends on the index n that has only a small dispersion. A classical quarter-wave ($\Lambda/4$) plate using a birefringent crystal, creates an optical path difference ΔL_{opt}, and not a phase retardation, *strictly speaking*. This path delay does yield a phase retardation $\Delta\varphi$, but this retardation is inversely proportional to the wavelength λ, since $\Delta\varphi = 2\pi \cdot \Delta L_{\mathrm{opt}}/\lambda$, as it is well-known.

The origin of stress-induced birefringence is complicated too. The highly-doped core is under tensile stress, as what we saw in the previous section for the SAPs of PM fibers (Fig. 19), while there is also some compressive stress in the surrounding cladding. With a circular core, the stresses are isotropic, but it is not the case anymore with an elliptical shape, which induces birefringence. To be honest, the theory of this effect is not clear to us ... and it is not clear in the literature. It will require some more analysis.

In any case, the total phase birefringence is very dispersive as confirmed by measurements at various wavelengths by Urbanczyk and co-workers [31]. On our side, we performed measurement of group birefringence over a wide spectrum (1000–1650 nm), and we deduced phase birefringence with a single wavelength measurement, as what we did for the PM fibers with SAPs, seen in the previous section (Fig. 23). The elliptical core has a major-axis $2a$ width of 4 μm and a minor-axis width $2b$ of 2 μm; the cut-off

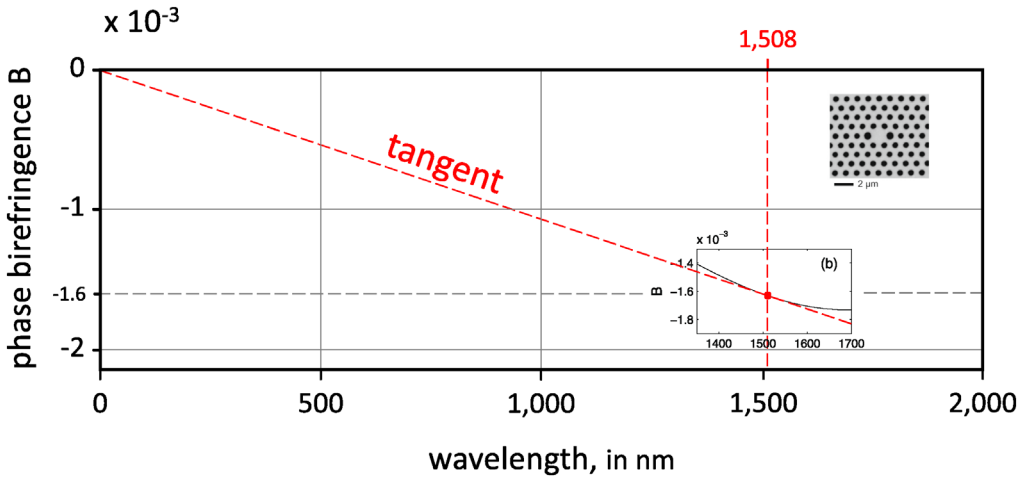

Figure 26. *Revisited* Figure 1b of [34]: the tangent to phase birefringence curve $B(\lambda)$ does cross at zero the *zero-wavelength* ordinate axis, for 1508 nm, where group birefringence is cancelled; the insert shows the shape of the micro-structured solid-core PM fiber described in [34], that has less anisotropy than the one described in [32], and Figure 24.

wavelength λ_c is 1050 nm for an operating wavelength of 1300 nm; the numerical aperture (NA) is 0.27, i.e., a core index step of 0.025; the cladding diameter is 80 µm. It is confirmed that phase-birefringence dispersion is very high, which yields a big difference between group and phase birefringences. At the operating wavelength of 1300 nm, B is only 2.3×10^{-4}, while B_g is 5.8×10^{-4}, i.e., 2.5 times bigger. We directly checked this big difference with an additional Bragg grating at 1300 nm to confirm it.

Finally, as described by Mélin and co-workers [32], shape birefringence is also found in solid-core micro-structured PM fiber, where there is a very strong phase birefringence: few 10^{-3}, when it is typically 5×10^{-4} in classical PM fibers. There is also an interesting effect: the value of phase birefringence dispersion $\mathrm{d}B/\mathrm{d}\lambda$ is very high, and it is *positive*, i.e., *anomalous* [1]. With the geometrical construction that was discussed in Figure 13, it is easy to see that group birefringence can become negative! Slow and fast modes are inverted, between phase birefringence and group birefringence. *Revisiting* Figure 3 of [32], phase birefringence at 1550 nm is about 3.6×10^{-3}, and phase-birefringence dispersion $\mathrm{d}B/\mathrm{d}\lambda$ is about 5×10^{-3} µm^{-1}; using (35), one finds a group birefringence B_g of *minus* 4.15×10^{-3} (Fig. 24). *Worth to outline,* isn't it?

It is also worth to outline that the shape birefringence of such solid-core micro-structured PM fibers can be *engineered* to get *cancellation* of group birefringence at a specific wavelength, as described by Morin and co-workers [33], and Kibler and co-workers [34]. Their figures can be *revisited* as well, and this confirms that the tangent to the phase birefringence curves $B(\lambda)$ does crosse at zero the ordinate axis corresponding to $\lambda = 0$, when group birefringence B_g is cancelled (Figs. 25 and 26). The slopes are inverted, because these two papers defined phase birefringence as negative, which is just a matter of convention.

It is interesting to compare the result of [32], revisited in Figure 24, with the one of [34], revisited in Figure 26. As seen in the inserts, the anisotropy of the shape of the micro-structured solid-core PM fiber of [34] is smaller than the one of [32], which yields less phase birefringence B (1.65×10^{-3} instead of 3.4×10^{-3} @ 1.5 µm, in absolute values), and less phase birefringence dispersion $\mathrm{d}B/\mathrm{d}\lambda$, or B' (1.05×10^{-3} µm^{-1} instead of 5×10^{-3} µm^{-1} @ 1.5 µm, in absolute values). According to equation (35), the condition for nulling out $B_g(\lambda)$ is $\lambda \cdot B'(\lambda) = B(\lambda)$, i.e., the *relative* phase birefringence dispersion $B'(\lambda)/B(\lambda)$ equates $1/\lambda$. This relative phase birefringence dispersion $B'(\lambda)/B(\lambda)$ is $1/(1.508\ \mu\mathrm{m}) = 0.663\ \mu\mathrm{m}^{-1}$ for [34], where $B_g(1.508\ \mu\mathrm{m}) = 0$, while it is $1.47\ \mu\mathrm{m}^{-1}$ for [32], which is more than twice higher. Then, group birefringence B_g goes beyond zero. It gets an opposite sign, and a larger absolute value than phase birefringence B. It is clear that obtaining the adequate design to null out group birefringence is complicated, but the *visual* geometrical construction *with the tangent* still applies and eases the understanding, even if you are not familiar, as us, with *cross-phase-modulation-instability band gap.*

9 Conclusion

This paper is a complement to an earlier JEOS-RP publication [1]. It presents comments and a *reversed* geometrical construction that should ease the understanding of birefringence dispersion in PM fibers. It also gives measurements of group birefringence $B_g(\lambda)$ and phase birefringence $B(\lambda)$ of several kinds of PM fibers. The points to remember are:

- The easy technique of measurement of birefringence is *channeled spectrum analysis* with a broadband source and an OSA, but it is *inherently* a group measurement, as outlined very early by Rashleigh [2].
- Phase birefringence $B(\lambda)$ over a wide spectrum is more complicated, but it can be retrieved from group birefringence $B_g(\lambda)$ over this wide spectrum, and a *single-wavelength* measurement $B(\lambda_0)$, with a simple geometrical construction.

- Birefringence dispersion is low in stress-induced PM fibers (bow-tie, panda, or tiger-eye), but not completely negligible for certain applications: the difference between B_g and B is about 15–20%, and group birefringence dispersion $dB_g/d\lambda$ is also significative. It is due, for a good part, to the decreasing of the stresses away from the core, but also to the intrinsic dispersion of photo-elasticity [2], which is not often mentioned.
- It is confirmed that birefringence dispersion is very high in elliptical-core (E-core) PM fibers: the difference between B_g and B can get up to a 3-fold factor.
- Shape birefringence in solid-core micro-structured fibers yields a surprising result: phase birefringence dispersion $dB/d\lambda$ is very high and positive, which can lead to a group birefringence B_g with an opposite sign! It is also possible to *engineer* the design to *cancel out* group birefringence at a specific wavelength.
- The use of the beat length @ 633 nm, to specify the strength of the birefringence, should be avoided when 633 nm is not the operating wavelength.
- To us, the concept of group birefringence is easier to grasp than the one of intrinsic-PMD, even if they are obviously related.

We hope that this paper will be useful and help to simplify the subject, knowing that seminal publications are not always easy to understand, if only because of the evolution of vocabulary over four decades.

References

1 Lefèvre H.C. (2022) Comments about dispersion of light waves, *J. Eur. Opt. Soc.: Rapid Publ.* **18**, 1. https://doi.org/10.1051/jeos/2022001.
2 Rashleigh S.C. (1983) Measurement of fiber birefringence by wavelength scanning, *Opt. Lett.* **8**, 6, 336–338.
3 Stolen R.H., Ramaswamy V., Kaiser P., Pleibel W. (1978) Linear polarization in birefringent single-mode fibers, *Appl. Phys. Lett.* **33**, 8, 669–701.
4 Snitzer E., Ostenberg H. (1961) Observed dielectric waveguide modes in the visible spectrum, *J. Opt. Soc. Am.* **51**, 499–505.
5 Rashleigh S.C., Stolen R.H. (1984) Status of polarization-preserving fibers, in: *Conference on Lasers and Electro-Optics, Anaheim, California, USA, 19–21 June 1984*, OSA Technical Digest, Paper WH4.
6 Stolen R.H., Rashleigh S.C. (1985) Polarization-holding fibers, in: *Optical Fiber Sensors Conference, San Diego, California, USA, 13–14 February 1985*, OSA Technical Digest, paper ThCC1.
7 Noda J., Okamoto K., Sasaki Y. (1986) Polarization-maintaining fibers and their applications, *J. Lightwave Technol.* **LT-4**, 8, 1071–1089.
8 Papp A., Harms H. (1975) Polarization optics of index-gradient optical waveguide fibers, *Appl. Opt.* **14**, 10, 2406–2411.
9 Rashleigh S.C. (1982) Wavelength dependence of birefringence in highly birefringent fibers, *Opt. Lett.* **7**, 6, 294–296.
10 Kikuchi K., Okoshi T. (1983) Wavelength-sweeping technique for measuring the beat length of linearly birefringent fibers, *Opt. Lett.* **8**, 2, 122–123.
11 Born M., Wolf E. (1999) *Principles of Optics*, 7th ed., Cambridge University Press, Sub-section 7.3.3, pp. 295–296.
12 Okoshi T. (1981) Single-polarization single-mode optical fibers, *IEEE J. Quantum Electron.* **QE-17**, 6, 879–884.
13 Birch R.D., Payne D.N., Varnham M.P. (1982) Fabrication of polarisation-maintaining fibres using gas-phase etching, *Electron. Lett.* **18**, 24, 1036–1038.
14 Takada K., Noda J., Okamoto K. (1986) Measurement of spatial distribution of mode coupling in birefringent polarization-maintaining fiber with new detection scheme, *Opt. Lett.* **11**, 10, 680–682.
15 Lefèvre H.C. (1987) Comments about the fiber-optic gyroscope, *SPIE Proc.* **838**, 86–97.
16 Martin P., Le Boudec G., Lefèvre H.C. (1991) Test apparatus of distributed polarization coupling in fiber gyro coils using white light interferometry, *SPIE Proc.* **1585**, 173–179.
17 Yao X.S. (2019) Techniques to ensure high-quality fiber optic gyro coil production, in: Udd E., Digonnet M. (eds), *Design and Development of Fiber Optic Gyroscopes, Chapter 11*, SPIE Press, pp. 217–261.
18 Lefèvre H.C. (2022) Testing with optical coherence domain polarimetry (OCDP), or today, distributed polarization cross-talk analysis (DPXA), in: *The Fiber-Optic Gyroscope*, 3rd ed., Artech House, Sub-section 5.4, pp. 110–123.
19 Simon A., Ulrich R. (1977) Evolution of polarization along a single-mode fiber, *Appl. Phys. Lett.* **31**, 8, 517–520.
20 Takada K., Noda J., Ulrich R. (1985) Precision measurement of modal birefringence of highly birefringent fibers, *Appl. Opt.* **24**, 24, 4387–4391.
21 Calvani R., Caponi R., Cisternino, F., Coppa G. (1987) Fiber birefringence measurement with an external stress method and heterodyne polarization detection, *J. Light. Technol.* **LT-5**, 9, 1176–1182.
22 Bock W.J., Urbanczyk W. (1993) Measurement of polarization mode dispersion and modal birefringence in highly birefringent fibers by means of electronically scanned shearing-type interferometry, *Appl. Opt.* **32**, 30, 5841–5848.
23 Shlyagin M.G., Khomenko A.V., Tentori D. (1995) Birefringence dispersion measurement in optical fibers by wavelength scanning, *Opt. Lett.* **20**, 8, 869–871.
24 Kashyap R. (2010) *Fiber Bragg Gratings*, 2nd ed., Academic Press.
25 Froggatt M.E., Gifford D.K., Kreger S., Wolfe M., Soller B.J. (2006) Characterization of polarization-maintaining fiber using high-sensitivity optical-frequency-domain reflectometry, *J. Light. Technol.* **24**, 11, 4149–4154.
26 Eickhoff W., Ulrich R. (1981) Optical frequency domain reflectometry in single-mode fiber, *App. Phys. Lett.* **39**, 9, 694–695.
27 Sinha N.K. (1978) Normalized dispersion of birefringence of quartz and stress optical coefficient of fused silica and plate glass, *Phys. Chem. Glass.* **19**, 4, 69–77.
28 Shibata N., Okamoto K., Tateda M., Seikai S., Sasaki Y. (1983) Modal birefringence and polarization mode dispersion in single-mode fibers with stress-induced anisotropy, *IEEE J. Quant. Electron.* **QE-19**, 6, 1110–1115.
29 Poole C.D. (1989) Measurement of polarization-mode dispersion in single-mode with random mode coupling, *Opt. Lett.* **14**, 10, 523–525.
30 Kumar A., Ghatak A. (2011) Elliptical-core fibers SPIE Tutorial, in: *Polarization of light with applications in optical fibers*, vol. **TT90**, SPIE Tutorial Text, Sub-section 9.2.1.1, pp. 171–175.

31 Urbanczyk W., Martynkien T., Bock W.J. (2001) Dispersion effects in elliptical-core highly birefringent fibers, *Appl. Opt.* **40**, 12, 1911–1920.

32 Mélin G., Cavani O., Gasca L., Peyrilloux A., Provost L., Rejeaunier X. (2003) Characterization of a polarization maintaining microstructured fiber, in: ECOC-IOOC Proceedings, Rimini, Italy, AEI, September 21–25, vol. **3**, Paper We1.7.4.

33 Morin P., Kibler B., Fatome J., Finot C., Millot G. (2010) Group birefringence cancellation in highly birefringent photonic crystal fibre at telecommunication wavelengths, *Electron. Lett.* **46**, 7, 525–526.

34 Kibler B., Amrani F., Morin P., Kudlinski A. (2016) Cross-phase-modulation-instability band gap in a birefringence-engineered photonic-crystal fiber, *Phys. Rev. A* **93**, 013857-1–013857-7.